

UNCLASSIFIED

AD NUMBER
AD915842
NEW LIMITATION CHANGE
TO Approved for public release, distribution unlimited
FROM Distribution authorized to U.S. Gov't. agencies only; Test and Evaluation; 10 JAN 1974. Other requests shall be referred to Director, USA Ballistic Research Laboratories, ATTN: AMXBR-SS, Aberdeen Proving Ground, MD 21005.
AUTHORITY
USAARDC ltr dtd 8 Mar 1978

THIS PAGE IS UNCLASSIFIED

BRL MR 2337

# BRL

AD

MEMORANDUM REPORT NO. 2337

## VERIFICATION OF GROUND TEST DATA BY INSTRUMENTED FLIGHT TEST OF AN ARTILLERY SHELL

by

V. Oskay  
J. H. Whiteside  
S. Kahn

DDC  
RECEIVED  
JAN 10 1974  
RECEIVED  
C

October 1973

Distribution limited to US Government agencies only. 10 JAN 1974  
Other requests for this document must be referred to  
Director, USA Ballistic Research Laboratories, ATTN: T&E  
AMXBR-SS, Aberdeen Proving Ground, Maryland 21005.

AD 915842

USA BALLISTIC RESEARCH LABORATORIES  
ABERDEEN PROVING GROUND, MARYLAND

Destroy this report when it is no longer needed.  
Do not return it to the originator.

Secondary distribution of this report by originating  
or sponsoring activity is prohibited.

Additional copies of this report may be obtained  
from the Defense Documentation Center, Cameron  
Station, Alexandria, Virginia 22314.

The findings in this report are not to be construed as  
an official Department of the Army position, unless  
so designated by other authorized documents.

BALLISTIC RESEARCH LABORATORIES

MEMORANDUM REPORT NO. 2337

OCTOBER 1973

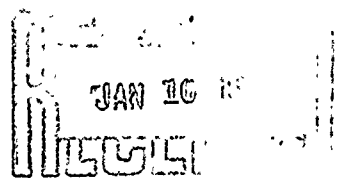
VERIFICATION OF GROUND TEST DATA BY  
INSTRUMENTED FLIGHT TEST OF AN ARTILLERY SHELL

V. Oskay  
J. H. Whiteside

Exterior Ballistics Laboratory

S. Kahn

U. S. Army Picatinny Arsenal



Distribution limited to US Government agencies only. 10 JAN 1974  
Other requests for this document must be referred to  
Director, USA Ballistic Research Laboratories, ATTN: 721  
AMXBR-SS, Aberdeen Proving Ground, Maryland 21005.

RDT&E Project No. 1T262301A201

ABERDEEN PROVING GROUND, MARYLAND

BALLISTIC RESEARCH LABORATORIES

MEMORANDUM REPORT NO. 2337

VOskay/JHWhiteside/SKahn/ds  
Aberdeen Proving Ground, Md.  
October 1973

VERIFICATION OF GROUND TEST DATA BY  
INSTRUMENTED FLIGHT TEST OF AN ARTILLERY SHELL\*

ABSTRACT

Service tests of a new low-drag projectile showed unexpected behavior at intermediate temperatures and low gun elevations where no problems were expected. An extensive test program was initiated to investigate the causes of this behavior. This program included wind tunnel and spark range tests at a wide range of Mach numbers and angles of attack. Given the shell's pitch damping, static, and highly non-linear Magnus moment coefficients, it was possible to predict its behavior mathematically if the initial pitching rate of the projectile was permitted to vary within the observed limits. Instrumented flight tests verified some of the ground test results although there still remains some unexplained discrepancies in the details of flight behavior. This investigation proved the necessity of a thorough aerodynamic test program if details of a shell's behavior are to be mathematically simulated.

---

*\*This paper has also been published as AIAA Preprint No. 72-979 in September 1972 and as an article in the Journal of Aircraft, Vol. 10, No. 3, March 1973, pp. 143-149.*

TABLE OF CONTENTS

	Page
ABSTRACT . . . . .	3
LIST OF ILLUSTRATIONS . . . . .	7
LIST OF SYMBOLS . . . . .	9
I. INTRODUCTION . . . . .	11
II. HISTORICAL BACKGROUND . . . . .	12
III. WIND TUNNEL AND SPARK RANGE TEST RESULTS . . . . .	13
A. Determination of Weapon/Projectile Interaction . . . . .	13
B. Determination of the Aerodynamic Coefficients . . . . .	14
IV. SIX-DEGREE-OF-FREEDOM, 6D, SIMULATIONS . . . . .	16
V. TEST RESULTS FROM INSTRUMENTED FLIGHTS . . . . .	18
VI. CONCLUSIONS . . . . .	19
REFERENCES . . . . .	39
DISTRIBUTION LIST . . . . .	41

LIST OF ILLUSTRATIONS

Figure	Page
1. Prototype for the New 155mm Shell Family . . . . .	21
2. Range Deviation Observed During Service Tests at Fort Sill . . . . .	22
3. First Maximum Yaw Distribution Observed at Aberdeen Proving Ground . . . . .	23
4. Mach Number Effect on Damping Factors . . . . .	24
5. Yaw Effect on Nutational Damping Factor . . . . .	25
6. Mach Number/Reynolds Number Regime of Wind Tunnel Tests. . .	26
7. Mach Number Variation of Drag Coefficient. . . . .	27
8. Yaw Effect on Static Moment Coefficient at Mach Number 0.7 .	28
9. Mach Number Trend of Static Moment Coefficient Slope . . . .	29
10. Mach Number Dependence of Pitch Damping Moment Coefficient .	30
11. Spin Effect on Magnus Moment Coefficient at Mach Number 0.7 and Test Reynolds Number $0.82 \times 10^6$ per caliber . . . . .	31
12. Reynolds Number Effect on Magnus Moment Coefficient at Mach 0.7 and Non-Dimensional Spin Value 0.31 . . . . .	32
13. Mach Number Trend of Magnus Moment Coefficient Slope . . . .	33
14. Comparison of Computed Yawing Histories under Aberdeen Proving Ground Environment . . . . .	34
15. Comparison of Computed Yawing Histories under Yuma Proving Ground Environment . . . . .	35
16. Spin History of a Yawsonde Instrumented Projectile Tested at Wallops Island . . . . .	36
17. Spin Damping Coefficient Computed from Yawsonde Instrumented Projectile Tests . . . . .	37
18. Solar Aspect Angle History of a Yawsonde Instrumented Projectile Tested at Wallops Island . . . . .	38

## LIST OF SYMBOLS

- $C_D = \frac{\text{Drag Force}}{Q S}$  , drag coefficient
- $C_{\ell_p} = \frac{\text{Rolling Moment}}{Q d S (pd/V)}$  , roll moment coefficient (Positive coefficient increases the rolling rate.)
- $C_M = \frac{\text{Static Moment}}{Q d S}$  , static moment coefficient (Positive coefficient increases the angle of attack.)
- $C_{M_\alpha} = C_M / \sin \alpha_t$  , static moment coefficient slope
- $C_{M_p} = \frac{\text{Magnus Moment}}{Q d S (pd/V)}$  , Magnus moment coefficient (Positive coefficient rotates the nose of the model normal to the plane of total angle of attack in the roll direction.)
- $C_{M_{p\alpha}} = \text{Magnus moment coefficient slope}$
- $C_{M_q} = \frac{\text{Damping Moment}}{Q d S (q_t d/V)}$  , pitch damping coefficient (Positive coefficient increases the angular velocity of the model.)
- $C_N = \frac{\text{Normal Force}}{Q S}$  , normal force coefficient (Positive coefficient indicates a force in the total angle of attack plane and normal to the model axis in the positive direction of the total angle of attack.)
- $C_{N_p} = \frac{\text{Magnus Force}}{Q S (pd/V)}$  , Magnus force coefficient (Positive coefficient indicates a force perpendicular to normal force in the direction of the spin.)
- $C_{N_{p\alpha}} = \text{Magnus force coefficient slope}$
- d reference dimension (In this report the reference dimension is model diameter, ft.)
- g acceleration due to gravity, 32.2 ft/sec<sup>2</sup>

LIST OF SYMBOLS (continued)

- L length of model, ft.
- p spin rate of the model, rad/sec
- Q =  $\frac{1}{2}(\rho V^2/g)$ , dynamic pressure, lb/ft<sup>2</sup>
- q, r transverse angular velocities of the model, rad/sec (for most exterior ballistic uses  $q \doteq \dot{\alpha}$  and  $r \doteq -\dot{\beta}$ )
- $q_t$  =  $(q^2 + r^2)^{\frac{1}{2}}$
- $R_e$  =  $(\rho Vd/\mu g)$ , Reynolds number
- S Reference area (In this report the reference area is  $\pi d^2/4$ )
- V model velocity, ft/sec
- $\alpha, \beta$  angles of attack and side slip, respectively, rad
- $\alpha_t$  =  $(\alpha^2 + \beta^2)^{\frac{1}{2}}$ , total angle of attack, rad
- $\mu$  air viscosity, lb-sec/ft<sup>2</sup>
- $\rho$  air density, lb/ft<sup>3</sup>

## I. INTRODUCTION

The artilleryman has always desired to send a maximum payload as far as possible. In the past, the weapon designer met this requirement with long, large caliber guns. But the need of the modern army for greater mobility created a preference for shorter and more mobile howitzers or, when necessary, for medium length, intermediate caliber cannons. The previous requirements of artillery for longer ranges and heavier payloads have still remained. As a result, a major part of the burden shifted to the shell designer and the ballistician; their answer has been shell designs with larger internal volumes and/or more aerodynamically streamlined external surfaces. The resulting designs generally have: (a) long, ogival noses, (b) boattails, and (c) length-to-diameter ratios (L/d) greater than 5-1/2.

The gains in exterior and terminal ballistic performance were, however, achieved only at the expense of decreased gyroscopic and dynamic stability margins compared to those of the older shell designs. The aerodynamic property governing the gyroscopic stability of a projectile is the static moment which is relatively insensitive to spin and Reynolds number variation although yaw and Mach number effects can be large. On the other hand, the aerodynamic characteristics controlling the shell's dynamic stability are the pitch damping and Magnus moment coefficients which can be sensitive to all of the above variables and also to small changes in shape. The most critical conditions for the satisfactory behavior of these newer projectiles have been observed at transonic speeds where the Magnus moment is strongly influenced by yaw level and non-dimensional spin factor ( $\rho d/V$ ). Therefore, the testing necessary at transonic speeds can be expensive and time consuming if a thorough investigation is to be made. It should also be noted that only in recent years has the Magnus testing of wind-tunnel models become semi-routine for full scale Reynolds numbers at transonic speeds. Similarly, the spark ranges have only recently been able to produce and analyze large yaw data for full scale shells.

As of several years ago, only a small number of prototypes would be tested in a spark range at small yaw levels and a similarly small number would be fired under field conditions. The spark range results for the newer shell would almost certainly indicate marginal yaw damping somewhere within the expected region of launch velocities, usually at the transonic speeds, while the field tests often showed adequate precision at impact. Since it was nearly impossible to attempt a more comprehensive investigation, the development of the projectile usually proceeded, sometimes without the threat of misbehavior predicted by the spark range tests ever materializing. However, when it did, it was often at a late stage of the shell's development. A problem at this late stage necessitates attempting a field solution to avoid a redesign if possible; such a solution generally takes the form of changing or limiting the permissible muzzle velocities for the transonic launch conditions.

Recently, the prototype of a family of new shells encountered precision problems. The history of this projectile will be used to demonstrate: (a) the initial problems faced by the developers in the past, (b) the increase in the test capabilities with time, (c) the necessity for a comprehensive test program, (d) the degree to which the aerodynamic data could be used in trajectory simulations to duplicate the projectile's impact points, and finally (e) the extent to which the details of instrumented flight behavior could be used to verify and/or modify the aerodynamic data obtained from ground tests (wind tunnel and spark range tests).

## II. HISTORICAL BACKGROUND

The projectile, whose developmental history is described in this paper, is shown in Figure 1. It has a diameter of 0.5075 feet (155mm) and an (L/d) of 5.65. It has a 3-caliber long secant ogive and a 0.6 caliber, 7-1/2 degree boattail. During the initial design stages of this shell, estimates of linear aerodynamic coefficients were obtained from its similarity with previous shell designs. Although six-degree-of-freedom (6D) simulation using these linear coefficients showed that there could be precision problems for some transonic launch conditions, none were encountered during the developmental test firings at Yuma Proving Ground (YPG), Arizona for hot and normal temperature conditions and a small number of firings at Arctic Test Center (ATC), Alaska for cold temperature conditions, usually considered to be the most critical. Based on the success of these tests, the design was finalized and the service tests were started at Fort Sill, Oklahoma. During the service tests, large dispersions in the impact range, Figure 2, were detected at one muzzle velocity and a relatively low elevation angle where, in earlier testing, no problems had occurred. The range spread observed at Fort Sill could not be explained by round-to-round velocity variations and/or changes in wind; therefore, a more complicated condition had to exist. At Fort Sill, the air temperature was 28° C lower and the air density was 15% higher than was usual in the extensive YPG tests. Similar muzzle velocity, gun elevation, and atmospheric conditions were not encountered in any of the other, more limited, temperate and cold temperature tests. The service test behavior resulted in the initiation of a comprehensive program to determine: (a) the effect of launch conditions on range dispersion, (b) the effect of the observed differences in environmental conditions on the behavior of the shell at various test sites, and (c) the detailed aerodynamic properties of the projectile.

The specific investigations included: (a) open range tests with yaw camera coverage at Aberdeen Proving Ground (APG), Maryland to determine the effect of weapon/shell interaction on the initial flight of the projectile at weather conditions near those of the Fort Sill tests, (b) 6D analyses using the available aerodynamic data to determine

the effects of environmental conditions, (c) an extensive wind tunnel test program with a 0.7-scale model at several facilities to define the basic aerodynamic properties of the projectile, (d) a sizable (but not as extensive) test program of the full scale shell in the Ballistic Research Laboratories (BRL) spark range facility<sup>1\*</sup> at APG to confirm and augment the wind tunnel results, particularly at small yaw, and lastly (e) free-flight tests of projectiles instrumented with yawsondes at the Wallops Island facility of NASA to define its yawing behavior under actual flight conditions.

### III. WIND TUNNEL AND SPARK RANGE TEST RESULTS

Several parts of the test program discussed in this section had already been planned prior to the service tests. The observation of poor precision at Fort Sill, however, resulted in an augmentation of the already planned tests and in the addition of others. Although parts of the test program were carried out simultaneously for expediency, clarity is best served by explaining the various elements as if they occurred in a distinct sequential order.

#### A. Determination of Weapon/Projectile Interaction

Tests with yaw camera coverage were performed at APG and were the first intensive effort of their kind to determine weapon/shell interaction under a variety of conditions. These tests indicated that this weapon/shell system can yield sufficiently large shell pitching rates to result in sizable yawing motions after launch. Figure 3 shows the results of one such test. These tests uncovered the possibility of initial yaw levels exceeding  $8^\circ$  under the worst combination of launch speeds and meteorological conditions. These results formed the basis of the first attempts to explain the behavioral differences at different test sites.

It was possible using 6D simulations to predict those launch conditions which result in poor precision by using the initial yaw limits indicated in Figure 3 and the Fort Sill environment ( $9^\circ$  C air and propellant temperature and at least 5% higher air density than the ICAO standard atmosphere). However, the use of the linear aerodynamics available at the time did not yield a good representation of the ranges observed during the Fort Sill tests. A quasi-linear analysis of the shell's behavior, using some of the initial wind tunnel results, was performed to obtain a better understanding of the problem<sup>2</sup>. Under the Fort Sill conditions and at intermediate yaw levels (about  $4^\circ$ ), these analyses indicated that under the influence of a strong Magnus non-linearity as function of yaw the nutational component of the projectile's

---

*\*References are listed on page 37.*

yawing motion could become undamped, see Figure 4. These analyses further indicated that, in addition to the strong Mach number effect on the growth rate of the yawing motion as shown in Figure 4, the initial amplitude of the yaw will also influence the growth rate. The last result is clearly shown in Figure 5 for the nutational component at two Mach numbers. 6D analyses using the preliminary estimates of nonlinear aerodynamics partially explained the poor precision detected during Fort Sill tests as due to a combination of circumstances. These analyses also showed that the supposedly critical cold test firings would not have given rise to the problem. These details will be discussed later.

#### B. Determination of the Aerodynamic Coefficients

An extensive wind tunnel program was conducted with a 4.25-inch (108mm) diameter model at three test facilities<sup>3</sup> to define the aerodynamic characteristics of this projectile in greater detail. In addition to the normal force, static moment, Magnus force, and Magnus moment coefficients obtained during these tests, results of two earlier tests were used to give the trends of the drag and pitch damping coefficients where no data existed. Unfortunately, due to the operational limitations of the wind tunnels, most of the testing was performed at relatively low Reynolds numbers as shown in Figure 6. Since the Magnus characteristics of a boattailed projectile appear to be strongly influenced by the Reynolds number, a spark range program was also fired to obtain a reference for the full Reynolds number behavior of the shell at small yaws, especially at the critical transonic speeds. In this section, we will discuss some of these results and compare values of the aerodynamic coefficients obtained in the wind tunnel and spark range tests.

1. Drag Coefficient,  $C_D$ . The original estimates of the drag coefficient were obtained from a 105mm shell of similar shape<sup>4</sup>, modified at high supersonic Mach numbers by the results obtained from previous wind tunnel tests of a 1.2-inch model of similar shape. As the test program progressed, these estimates were revised by the results obtained in the BRL Transonic Range facility with the full size shell. Mach number trends of these three drag coefficients are shown in Figure 7. Also shown in the figure are some of the preliminary results for total drag obtained from the radar data of the instrumented shell tests.

2. Static Moment,  $C_M$ , and Normal Force,  $C_N$ , Coefficients. Static moment and normal force coefficients were measured in three different wind tunnel facilities. These tests were performed at various Mach numbers and angles of attack using a 4.25-inch model. Data were obtained at several Reynolds numbers with the non-spinning model. Figure 8 shows the variation of  $C_M$  as a function of angle of attack at a Mach number of 0.7 obtained in one of the wind tunnels. Also shown in the figure are several data points determined from the spark range tests.

It is obvious that the effect of Reynolds number on  $C_M$  is not very important. Figure 9 shows a comparison of the Mach number dependence of the static moment coefficient slope,  $C_{M\alpha}$ , at small angles (below  $3^\circ$ )

obtained from: (a) wind tunnel tests of 4.25-inch model, (b) spark range tests of the full-size projectile, and (c) a previous series of wind tunnel tests with a full-size model performed at AEDC<sup>5</sup>. Trends shown by the data from these three sources agree quite well although there are some differences in the absolute values of the coefficient, especially at subsonic Mach numbers, which may partially be explained by slight differences in ogive shape.

Dependence of the normal force coefficient on angle of attack, Mach number, and Reynolds number is quite similar to that of the static moment coefficient, and no additional discussion is needed.

3. Pitch Damping Moment Coefficient,  $C_{Mq}$ . The main source of data for the values of this coefficient was the spark range tests of the full size projectile. A plot of  $C_{Mq}$  as a function of Mach number is given in Figure 10. Also plotted are the data from the AEDC tests<sup>5</sup>. With the exception of low supersonic Mach numbers, where there is an oscillatory trend in the AEDC data, the agreement between the two curves is quite good. Analyses of the spark range data indicated that  $C_{Mq}$  is, at most, a weak function of angle of attack. For the computer simulations, this result was used as a basis for assuming the pitch damping to be independent of yaw.

4. Magnus Moment,  $C_{Mp}$ , and Magnus Force,  $C_{Np}$ , Coefficients. The values of the Magnus moment and force coefficients were determined mainly from the wind tunnel tests of the 4.25-inch model conducted at several Reynolds and Mach numbers<sup>3</sup>. The wind tunnel model was pre-spun by an air turbine and the data were recorded as the spin decayed. Several values of Magnus moment and force coefficient slopes ( $C_{Mp\alpha}$  and  $C_{Np\alpha}$ , respectively), were also determined during the spark range tests. In this section, only the Magnus moment behavior of the shell will be discussed since the influence of the Magnus force on the projectile's flight is, in general, minimal and the remarks made about  $C_{Mp}$  generally apply to  $C_{Np}$  too.

Figure 11 shows the effect of the spin rate on the value of  $C_{Mp}$ . The parameter  $(pd/V)$  is known as the non-dimensional spin and for a 1/20-

twist gun it has a value of 0.314 at the muzzle. As a projectile flies along its trajectory, the value of  $(pd/V)$  increases reaching a maximum near the summit. On the downleg of the trajectory,  $(pd/V)$  once more decreases. The wind tunnel results indicate that with increasing  $(pd/V)$ , the value of  $C_{M_p}$  decreases for yaw levels below  $10^\circ - 12^\circ$  as shown in

Figure 11 for a Mach number of 0.7 and a test Reynolds number of  $0.82 \times 10^6$  per caliber. After stall (above  $10^\circ - 12^\circ$  yaw levels), the trend appears to be reversed. In Figure 12, the effect of Reynolds number on  $C_{M_p}$  is shown for a Mach number of 0.7 and a non-dimensional spin rate of

0.31. The main effect of increasing Reynolds number is to decrease the value of  $C_{M_p}$ . This trend is in good agreement with spark range results,

also shown in Figure 12, at the full scale Reynolds number of  $2.51 \times 10^6$  per caliber. Another effect of increasing Reynolds number appears to be to accentuate the stall effect at yaw levels above  $10^\circ$ . Finally, a comparison of the values of Magnus moment coefficient slope,  $C_{M_{pa}}$ , obtained

during spark range tests and those derived from the wind tunnel tests is shown in Figure 13. Once more, the trends of spark range and wind tunnel results are in good agreement although at subsonic Mach numbers, the range values are again lower.

#### IV. SIX-DEGREE-OF-FREEDOM, 6D, SIMULATIONS

Using the new set of aerodynamic coefficients obtained by wind tunnel and spark range testing, further attempts were made to simulate the APG tests discussed above. These simulations were quite successful in matching the maximum range deviations observed during the APG tests although the maximum value of the initial yaw needed in the 6D analyses was generally lower than the observed values. This meant that either further refinements in the aerodynamic coefficients were needed or a choice had to be made between the values of first maximum yaw predicted by the 6D computations versus the photographically determined values during the APG tests. Additional 6D simulations were also performed with the YPG environmental conditions.

In Figures 14 and 15, we compare the results of four 6D trajectory simulations. The results of the analyses are presented as plots of total angle of attack versus time of flight. To compute the plots shown in Figure 14, the environmental conditions at APG (air temperature -  $7^\circ$  C and air density 11% above ICAO standard) were used since meteorological data for Fort Sill test were sketchy. Two rounds with the longest and the shortest ranges from one series of APG firings were chosen for simulation. An appropriate magnitude of initial pitching rate was used during the 6D simulation so that the computed range-to-impact matched the observed value. The same values of initial pitching rates were then

used in conjunction with the YPG environment (air temperature of  $42^{\circ}$  C and air density 11% lower than ICAO standard) to obtain the plots shown in Figure 15.

For the lower plot in Figure 14, only a small value of initial pitching rate was used thus resulting in a first maximum yaw of  $1.5^{\circ}$ . During the initial 2-3 seconds into the flight, the precessional component of the yaw is damped while the nutational component is growing. About half-way to the summit a region of neutral stability is reached and the yaw level remains constant at about  $2.5^{\circ}$ . Once the shell is over the summit, at about 12-13 seconds, the de-stabilizing effect of the plunging trajectory takes over and the nutational component of the yawing motion grows to a value of  $4.5^{\circ}$  at impact. The second plot in Figure 14 was computed with an initial pitching rate 7 times larger than the previous case. The resulting larger first maximum yaw (about  $8^{\circ}$  total angle of attack) has two consequences: (a) the nutational component of yaw grows at a faster rate than the previous case and (b) the precessional component takes a longer time to damp (there is still some perceptible precessional component at 8 seconds of flight). As a result, the total angle of attack reaches an average of about  $10^{\circ}$  at 3 seconds into the trajectory where the stabilizing effect of increasing altitude together with the damping precessional component tries to reduce the total yaw level. But by now, the nutational component is the dominant factor and the total yaw once more starts to grow even before the summital region (12-13 seconds of flight). On the downleg of the trajectory, the total yaw continues to grow but at a slower rate. From the plot, it appears as if the yawing motion of the projectile is approaching a limiting value of  $12^{\circ}$  -  $13^{\circ}$  at impact. This difference in the yawing behavior of the shell as a function of the amplitude of the initial pitching rate results in an increase in the average yaw level of about  $7.5^{\circ}$  along the complete trajectory for the higher pitching rate case. The resulting increase in the total drag of the shell is such that the flight with the larger initial pitching rate will have a range 620 meters shorter than the lower initial pitching rate flight.

In computing the plots of Figure 15, it was assumed that the environmental conditions of the test will not affect the interaction between the weapon and the shell; therefore, the pitching rates used to generate the plots of Figure 14 were also used to obtain the plots of Figure 15. The obvious difference between Figure 14 and 15 is that under YPG environmental conditions, for a given pitching rate, the shell has a first maximum yaw which is half as large as that for APG or Fort Sill environment. Consequently, at the reduced yaw, the motion either damps out completely or grows very slowly. This behavior is quite obvious in Figure 15. The low pitching rate flight has a first maximum yaw of about  $1^{\circ}$  which damps to about  $0.5^{\circ}$  and remains at that level for the entire flight. On the other hand, the 6D simulation using a higher pitching rate gives a first maximum yaw of about  $4.5^{\circ}$ . The precessional component of the yawing

motion damps during the first half of the trajectory while the nutational component remains at a level of about  $2^\circ$ . Once the shell is over the summit, the nutational component of the yawing motion starts growing. For this environmental condition, the growth rate of the nutational component is so slow that the projectile has an average yaw of only  $3^\circ$  at impact. Therefore, an average of  $1.5^\circ$  yaw difference exists between the two flights during the first half of the trajectory with the yaw difference reaching a maximum value of  $2.5^\circ$  at impact. The resulting difference in range could easily be masked by muzzle velocity, wind, and other usual test condition variations.

## V. TEST RESULTS FROM INSTRUMENTED FLIGHTS

There were two purposes in testing several yawsonde instrumented shells at the Wallops Island facility of NASA. One objective was to obtain first hand information on the yawing behavior of the projectile along its trajectory under critical environmental conditions. A second goal was to verify the spark range and wind tunnel test results either by simulating the motion of the instrumented flights using a 6D computation or by obtaining aerodynamic coefficients from these flights for comparison purposes. The yawsonde provides spin and yawing histories while total drag is obtained from radar data. A yawsonde is an instrument which employs a pair of solar cells to detect the position of the projectile axis with respect to the sun. This information is transmitted to a ground receiving station for analysis at a later date.

A small number of yawsonde instrumented shells were tested at Wallops Island in hopes of detecting the flight behavior under critical launch conditions. Because of the geographical location of Wallops Island, it was difficult to duplicate the exact launch conditions of the Fort Sill tests. Several rounds, however, were launched in the critical transonic regime. Preliminary data from one of these rounds will be discussed in this section.

The projectile under discussion was launched at a muzzle velocity of 1060 ft/sec (323 m/sec) with a gun elevation of 490 mils (27.5 degrees). The air temperature was  $57^\circ$  F ( $14^\circ$  C), and the air density was about 7% higher than ICAO standard. There was a tail wind of 14 miles/hour at an angle of  $26^\circ$  to the left of the trajectory.

The drag coefficient is the simplest aerodynamic coefficient to obtain. If wind and meteorological data are available, the total drag can be obtained from the radar data. Some preliminary results from this round are shown on Figure 7. There is greater scatter in the values of drag coefficient for this round than has been experienced in other radar reductions. In the present method, the drag variations due to yaw are superimposed on the normal data scatter. The technique of drag determination from positional radar data is still in its infancy and some lack of consistency is to be expected.

The second bit of information from the yawsonde instrumented shell is its spin history. Since each solar cell observes the sun once each revolution, the spin history is determined by counting the number of solar intercepts per unit time for a given cell. Such a plot is shown in Figure 16 for this flight. These data are analyzed for spin damping coefficient,  $C_{\dot{\alpha}_p}$ , as a function of Mach number. Figure 17 compares the values of  $C_{\dot{\alpha}_p}$  from the yawsonde data of this round with the data for a 105mm projectile of similar shape obtained during spark range testing<sup>4</sup>. Agreement between the two sets of data are quite good.

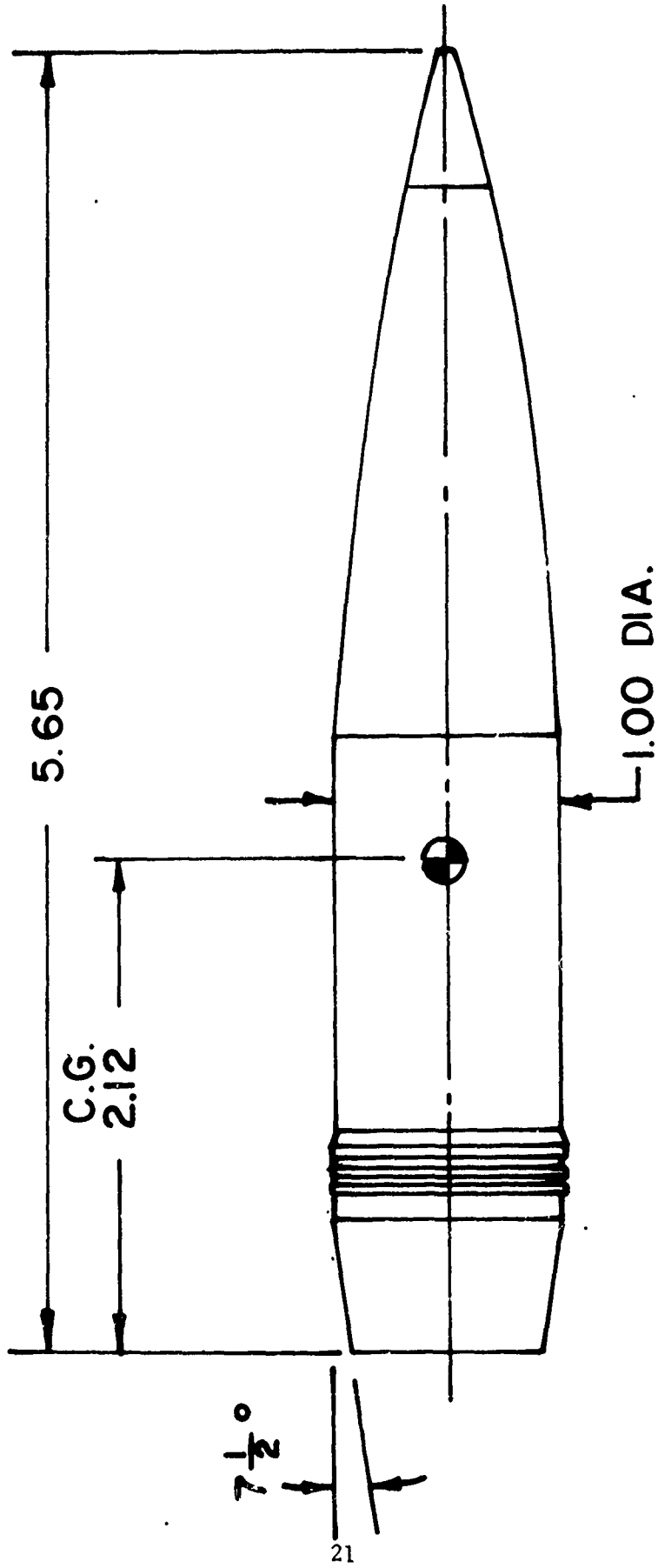
The last piece of information obtained during this test firing is the solar aspect angle history and is shown in Figure 18. The solar aspect angle is defined as the angle between the sun's ray and the normal to the shell's axis in the plane determined by the sun and the axis of symmetry of the projectile. The solar angle gives a general indication of the shell's behavior under particular test conditions. Data start at about one second into the trajectory (roughly 1000 feet from the muzzle) and show a combined yawing motion of about 7° peak-to-peak, a 4° nutational component superimposed on about a 2 - 2-1/2° precessional component. As the flight progresses towards the summit (between 14 and 15 seconds), the nutational component is damped but the precessional component persists. At the summit, there does not seem to be any perceptible motion. On the downleg portion of the trajectory, although the nutational component is quiescent, the precessional component is growing. This behavior does not agree with the predictions of 6D simulations using the aerodynamic coefficients determined from ground tests. The discrepancy may have several causes: (a) inadequate computer simulation of flight conditions, (b) simplifications made in the aerodynamics of the projectile (Reynolds number and spin effects are ignored although some measurements of these were made), and (c) inadequate description of the test conditions, particularly the wind. At the writing of this report, this problem is being studied from two approaches: (a) 6D simulations of the solar aspect angle history are being made to determine the extent of modifications needed in the aerodynamic coefficients and (b) the effective values of these coefficients are being determined from the details of the solar aspect angle history by solving the equations of motion. These two independent determinations of the coefficients would then be compared for further refinement.

## VI. CONCLUSIONS

Although some questions still remain about the details of the shell's aerodynamic behavior, the reasons for poor precision were quite adequately explained. This weapon/shell combination may result in first-maximum-yaw levels up to 8°. Under certain environmental conditions, this yaw will remain almost constant for the entire trajectory if the projectile is launched within the critical transonic regime. Based on the conclusions

drawn from the 6D analyses, it was possible to obtain a rational solution to the precision problem of this weapon/shell combination by eliminating the launch velocities at the critical region. The same nonlinear aerodynamic data package was also used to aid in the design of another member of this shell family meant for use with the same weapon system. Finally, when these aerodynamic coefficients were used in 6D analyses with APG environmental conditions, the actual test results were successfully simulated.

In general, it was found that the use of "linear" aerodynamic properties from small-yaw tests and the computations based on these tests may define regions where performance problems can be expected. Nevertheless, analyses based on "linear" aerodynamics do not define the behavior adequately enough to evaluate the severity of the problem. Furthermore, there now exists the capability to conduct an adequate test program to define a shell's behavior as a function of yaw level, Mach number, and spin rate so that detailed flight histories can be simulated by computer analyses. The most critical aerodynamic features needed to be measured are Magnus and pitch damping moment coefficients. Both wind tunnel and spark range tests are required for an adequate definition of the yaw dependence of the aerodynamic coefficients. Testing must be performed at essentially full flight Reynolds number at the critical regions of the flight regime. Launch conditions, particularly weapon/shell interactions, strongly influence the projectile's flight behavior when the stability of the shell is a nonlinear function of yaw. Finally, combinations of "field" conditions can produce considerably different launches from those usually observed during "proving ground" testing.



**ALL DIMENSIONS ARE IN CALIBERS**  
**ONE CALIBER IS 0.5075 FOOT**

Figure 1. Prototype for the New 155mm Shell Family

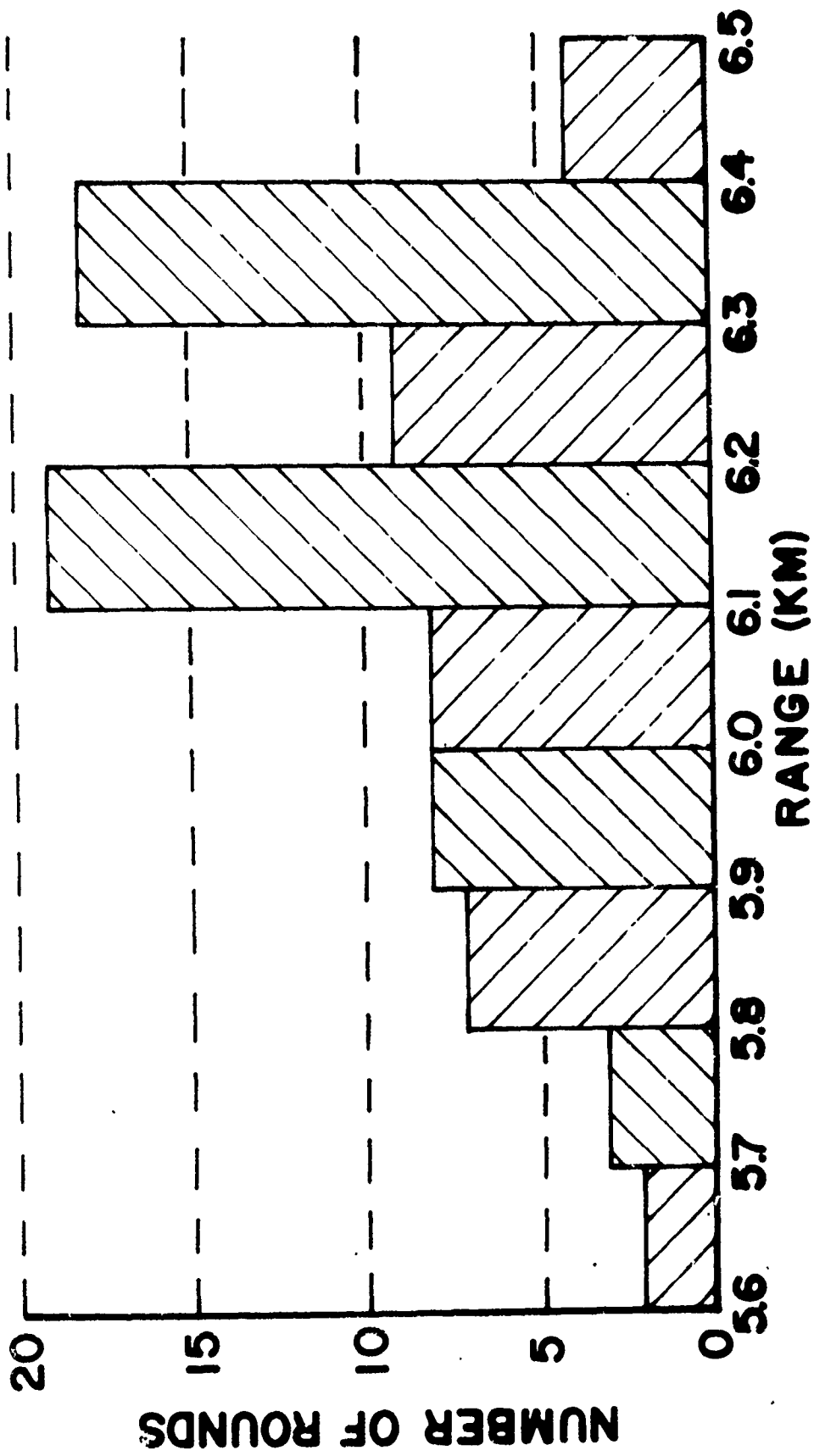
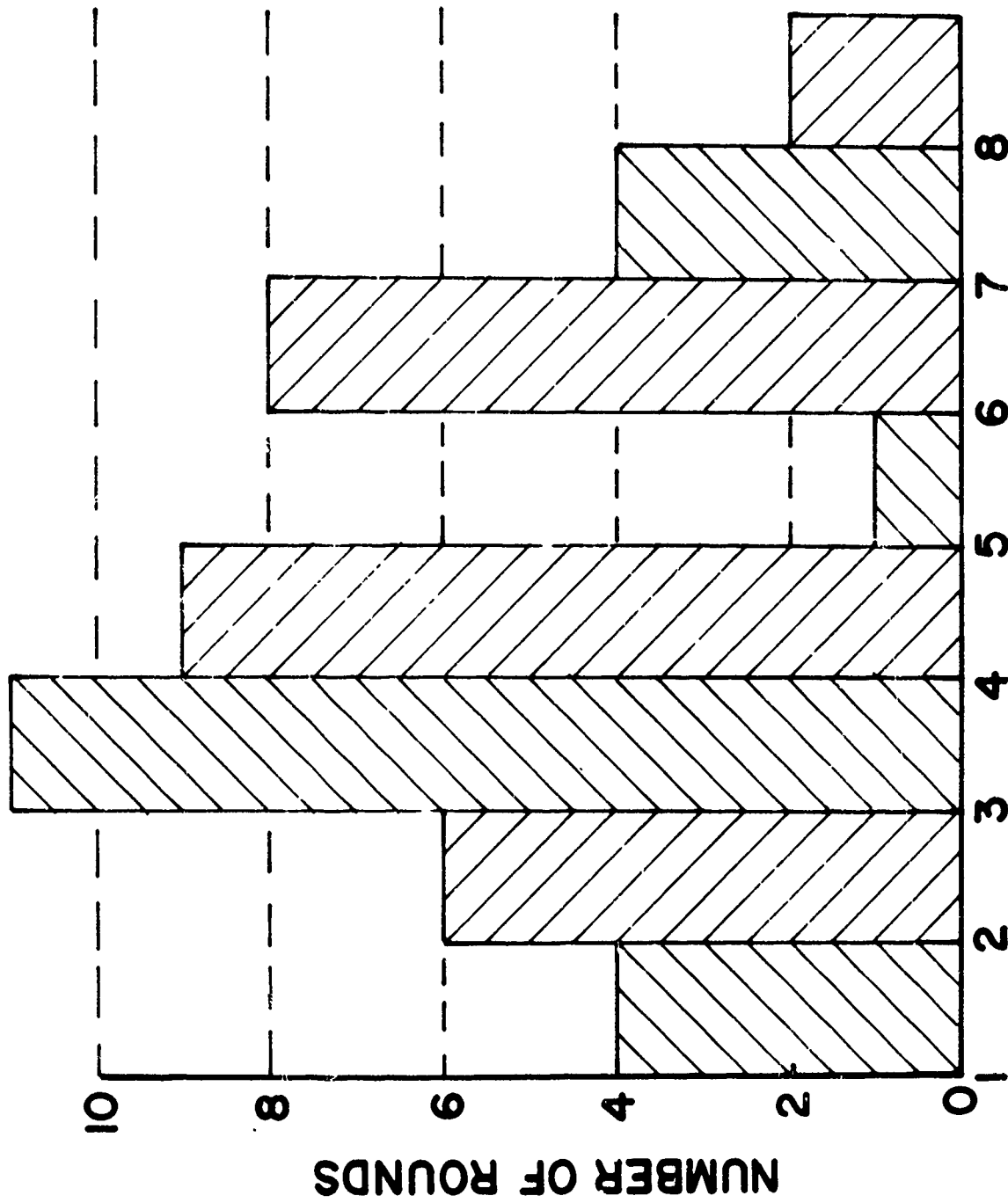


Figure 2. Range Deviation Observed During Service Tests at Fort Sill



**FIRST MAXIMUM YAW (DEGREES)**

Figure 3. First Maximum Yaw Distribution Observed at Aberdeen Proving Ground

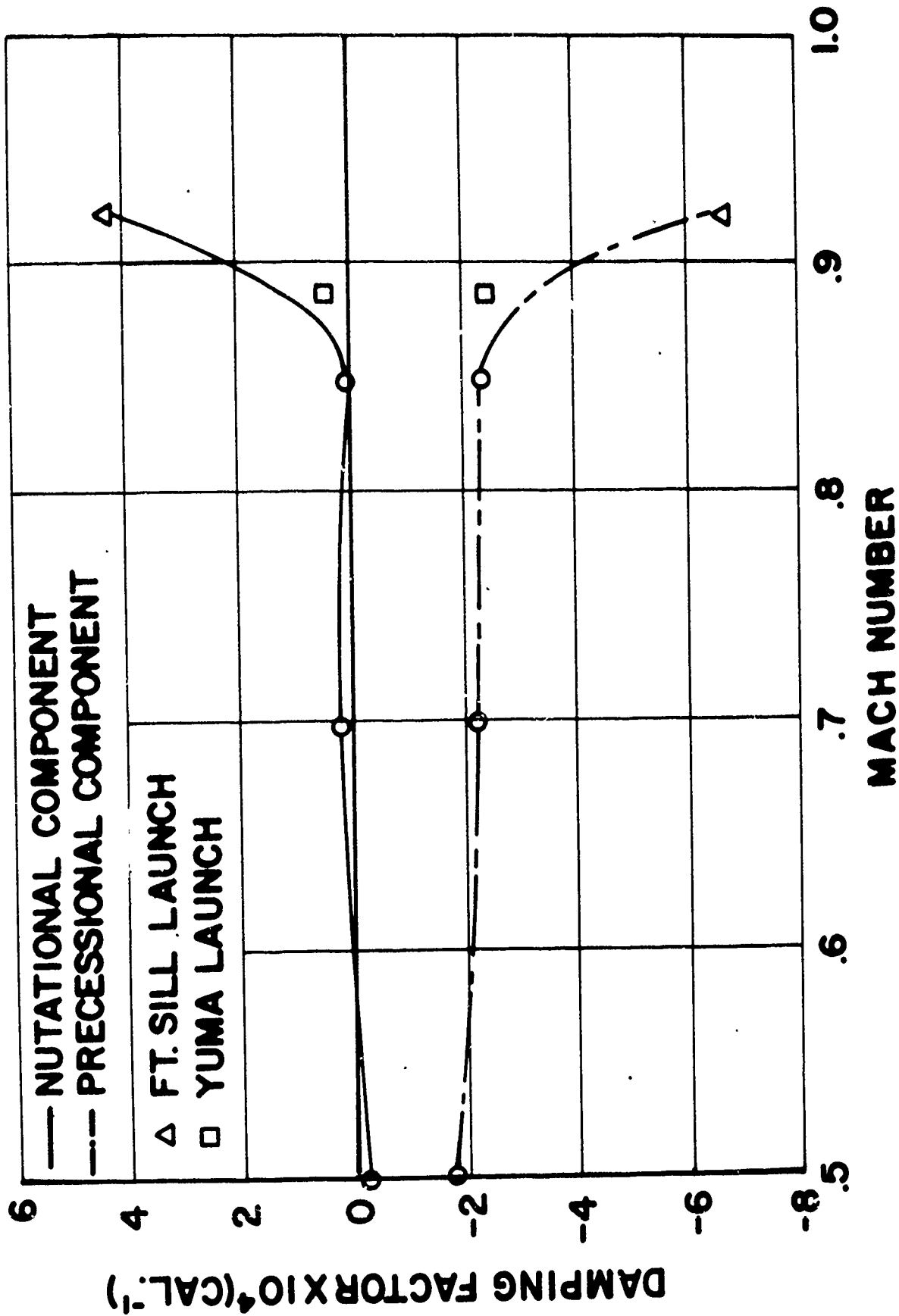


Figure 4. Mach Number Effect on Damping Factors

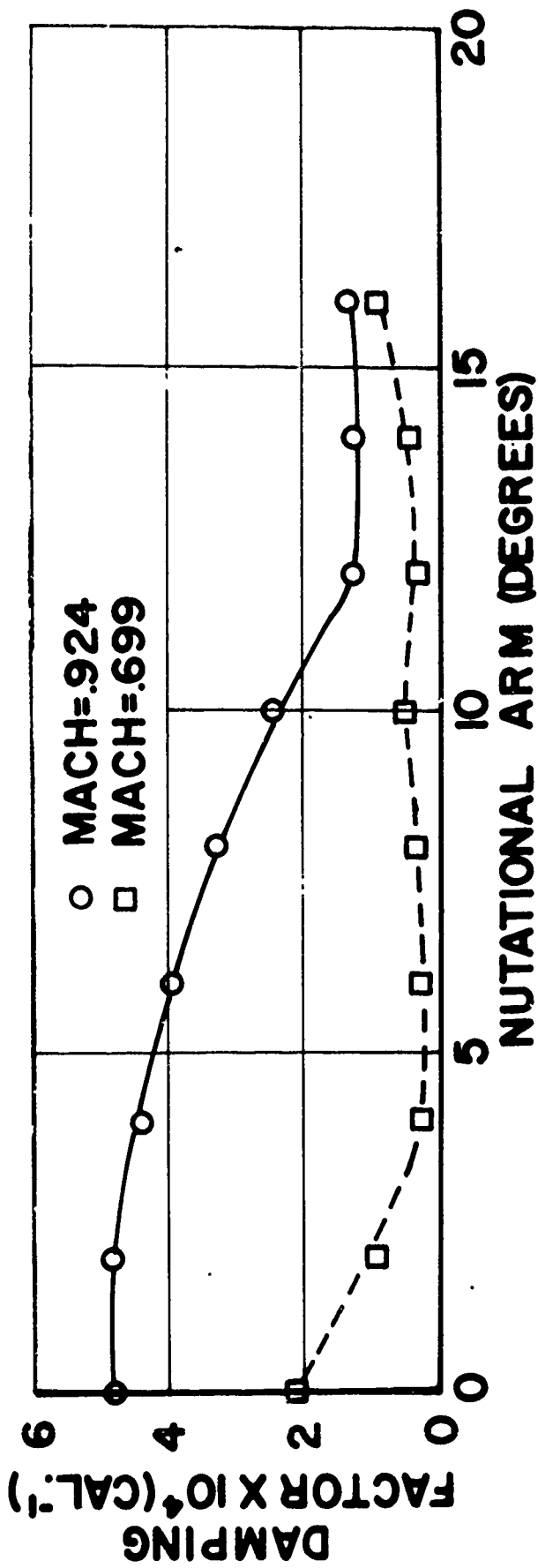


Figure 5. Yaw Effect on Nutational Damping Factor

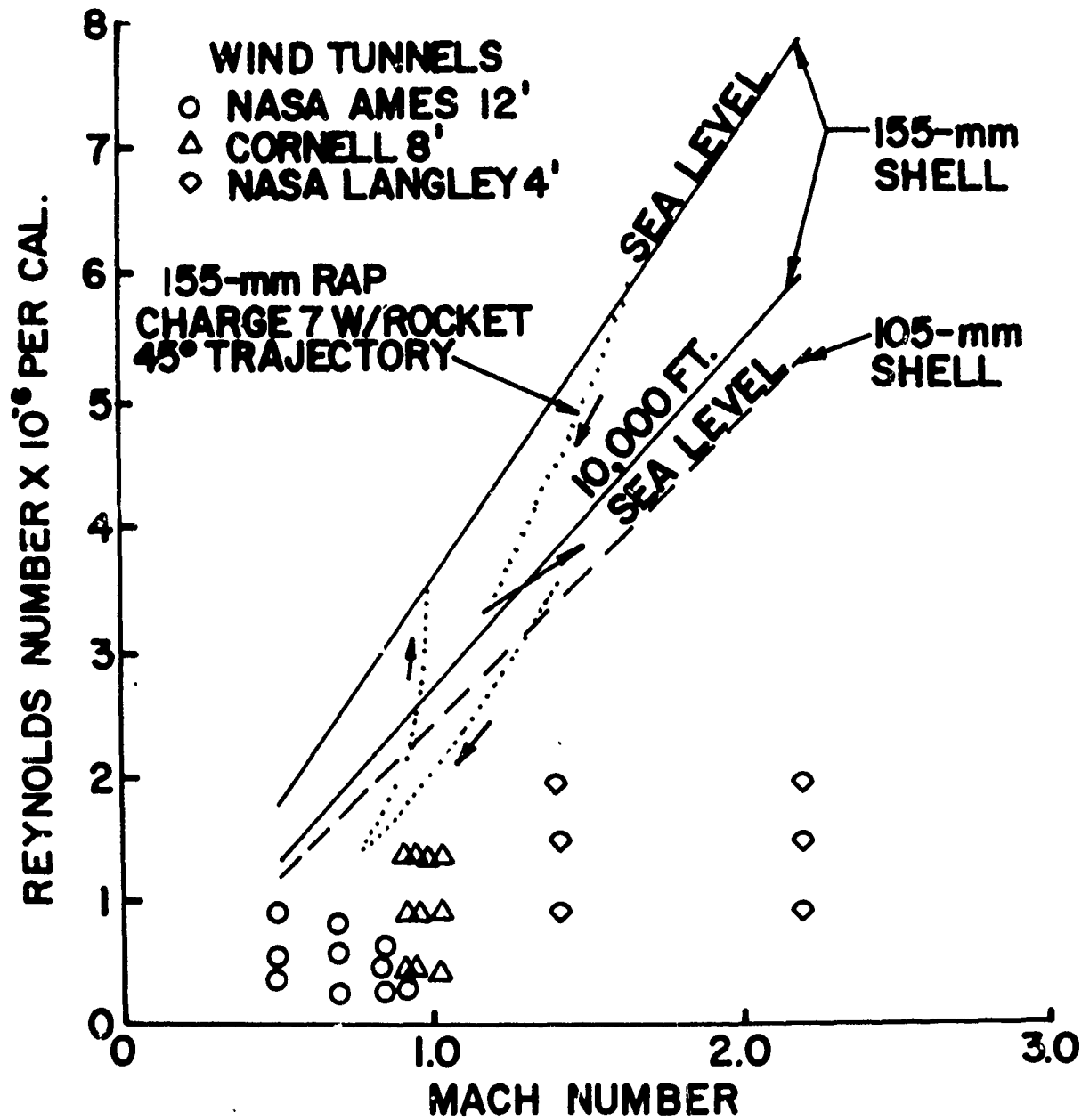


Figure 6. Mach Number/Reynolds Number Regime of Wind Tunnel Tests

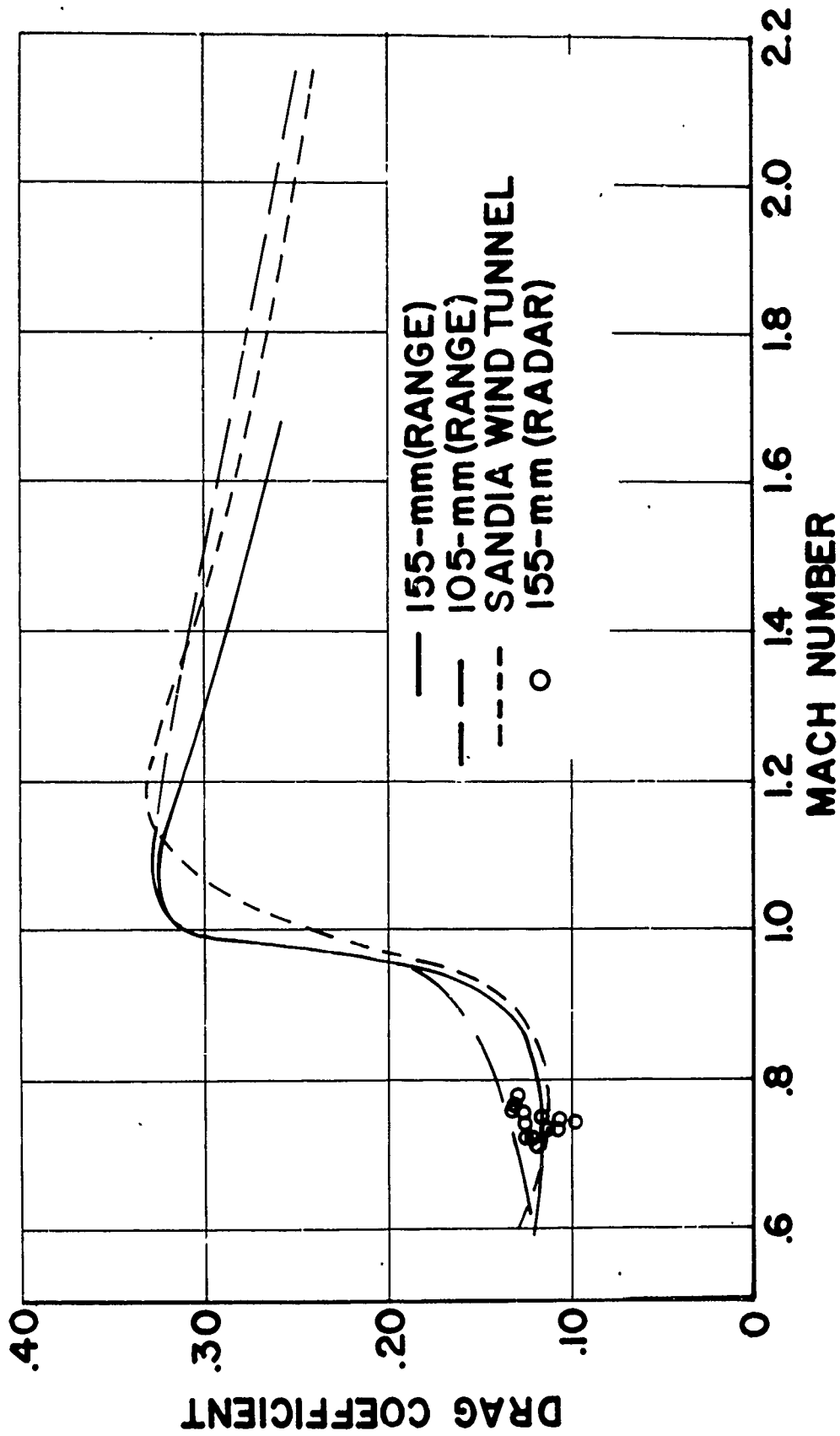


Figure 7. Mach Number Variation of Drag Coefficient

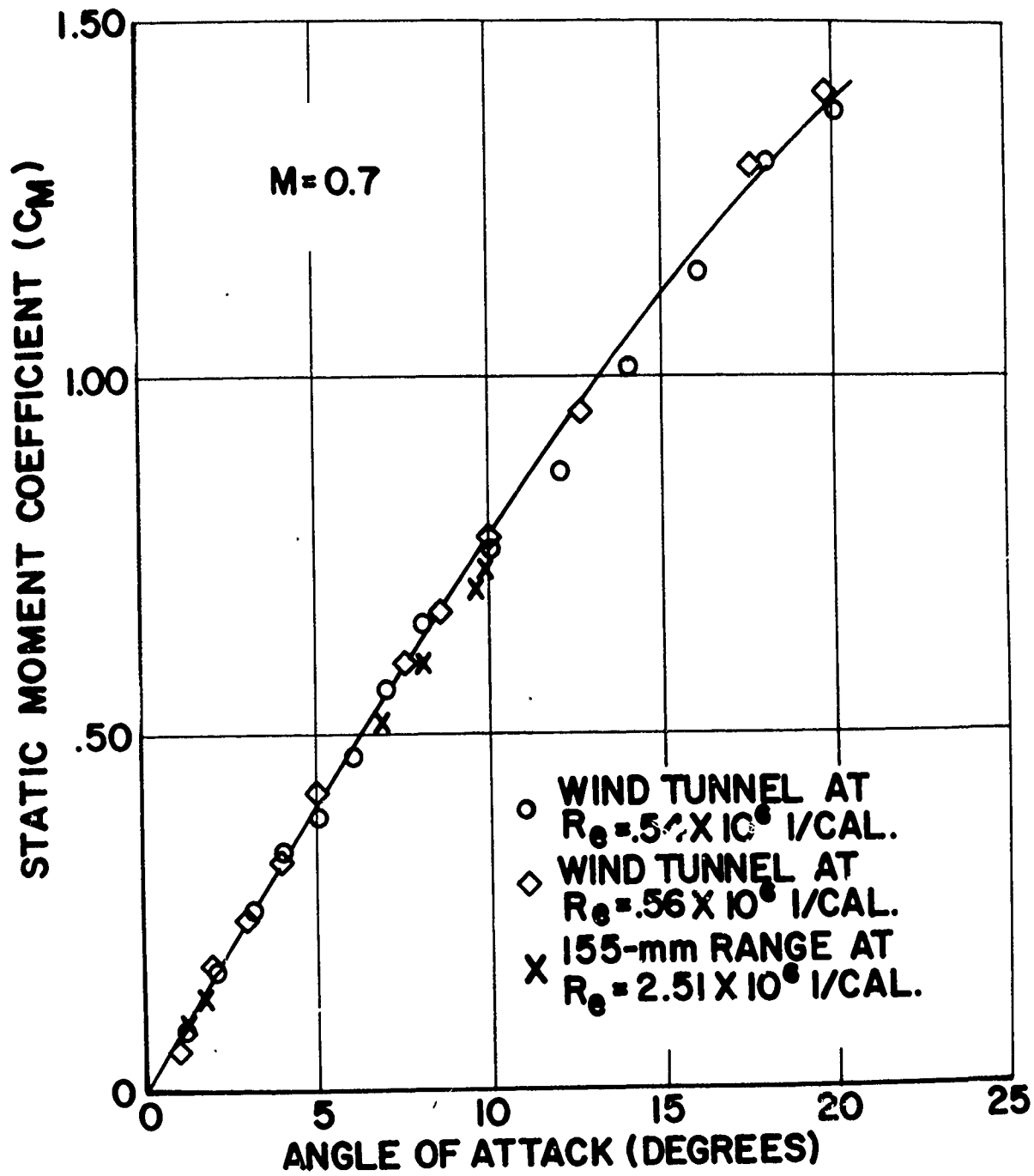


Figure 8. Yaw Effect on Static Moment Coefficient at Mach Number 0.7

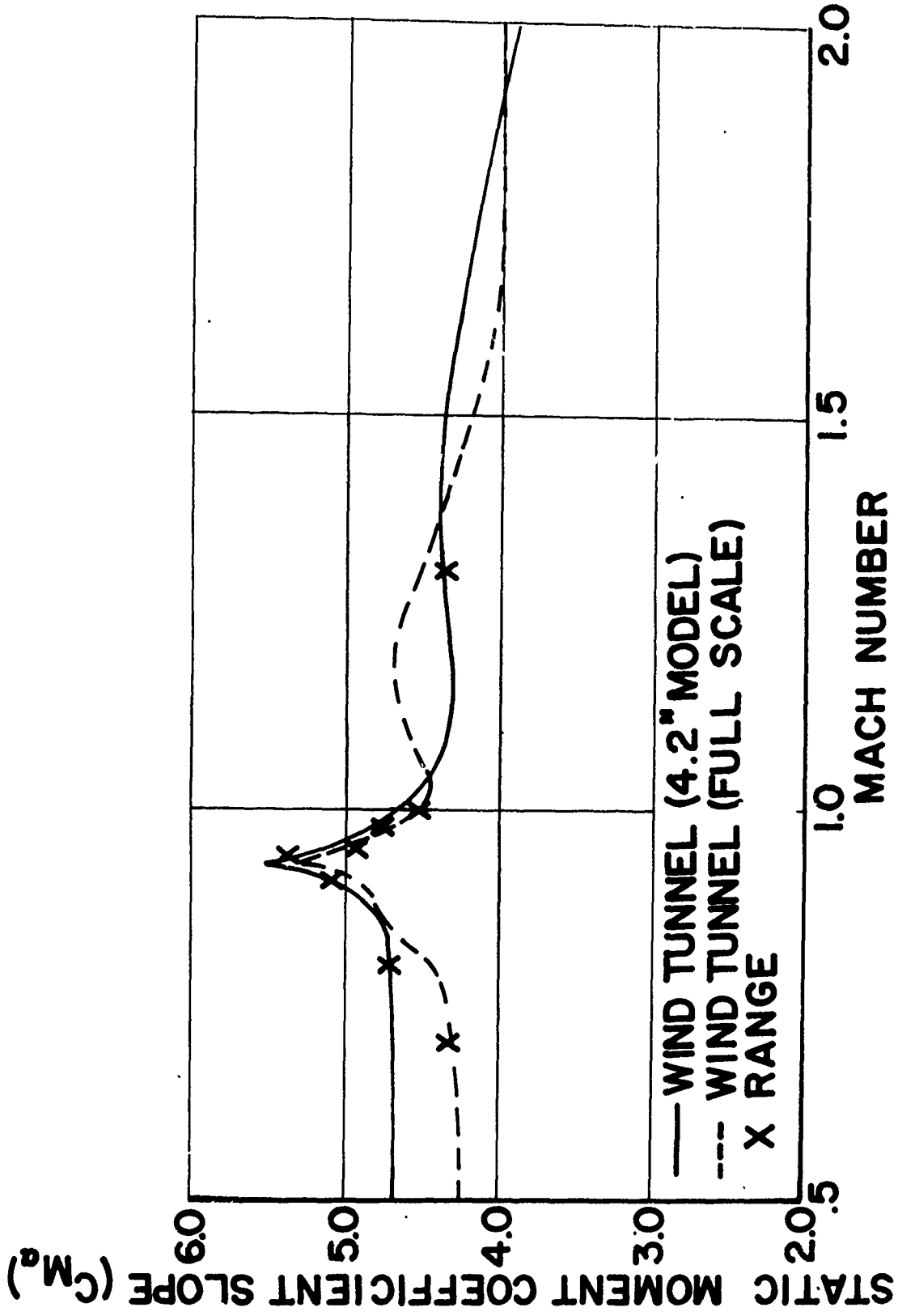


Figure 9. Mach Number Trend of Static Moment Coefficient Slope

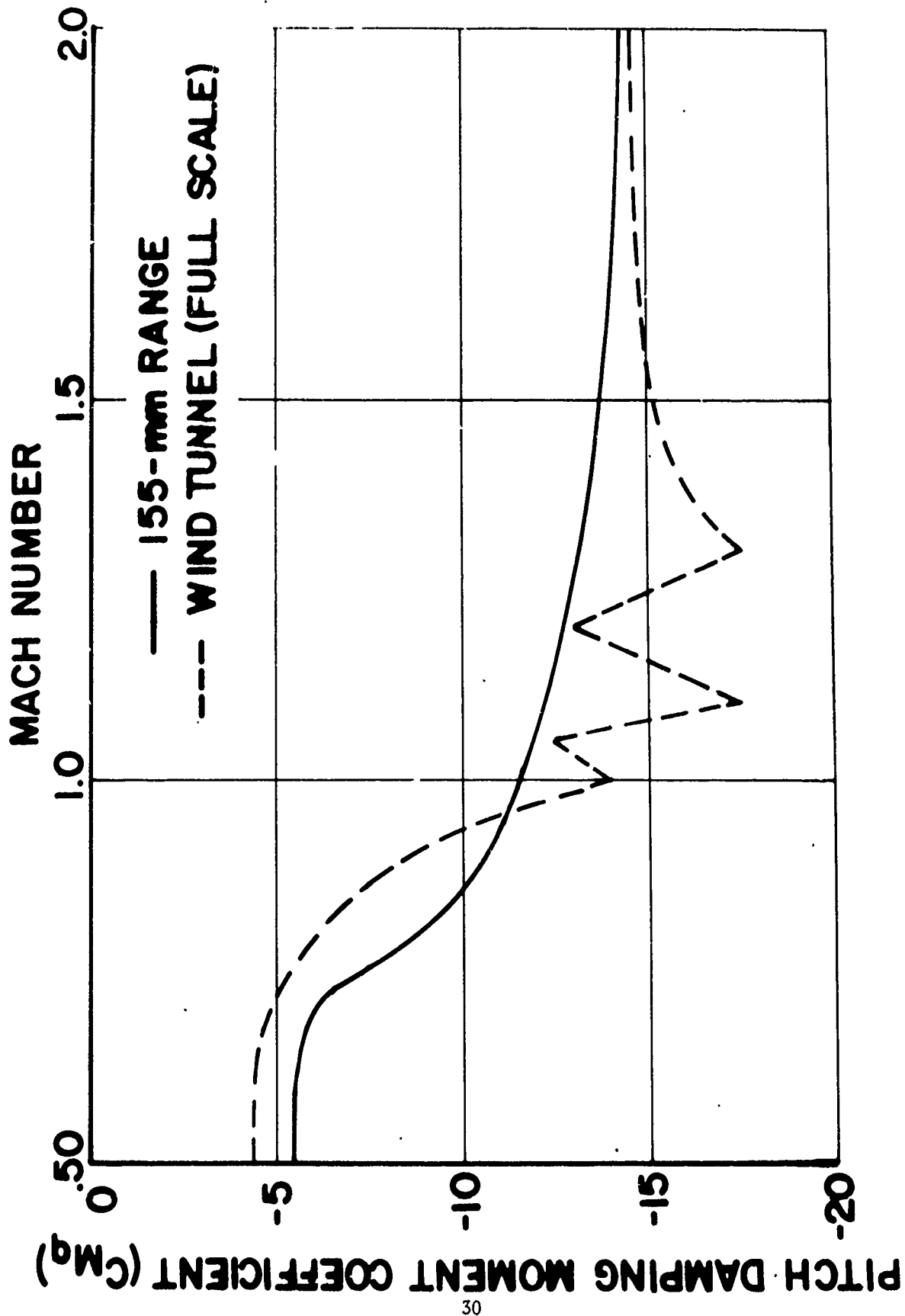


Figure 10. Mach Number Dependence of Pitch Damping Moment Coefficient

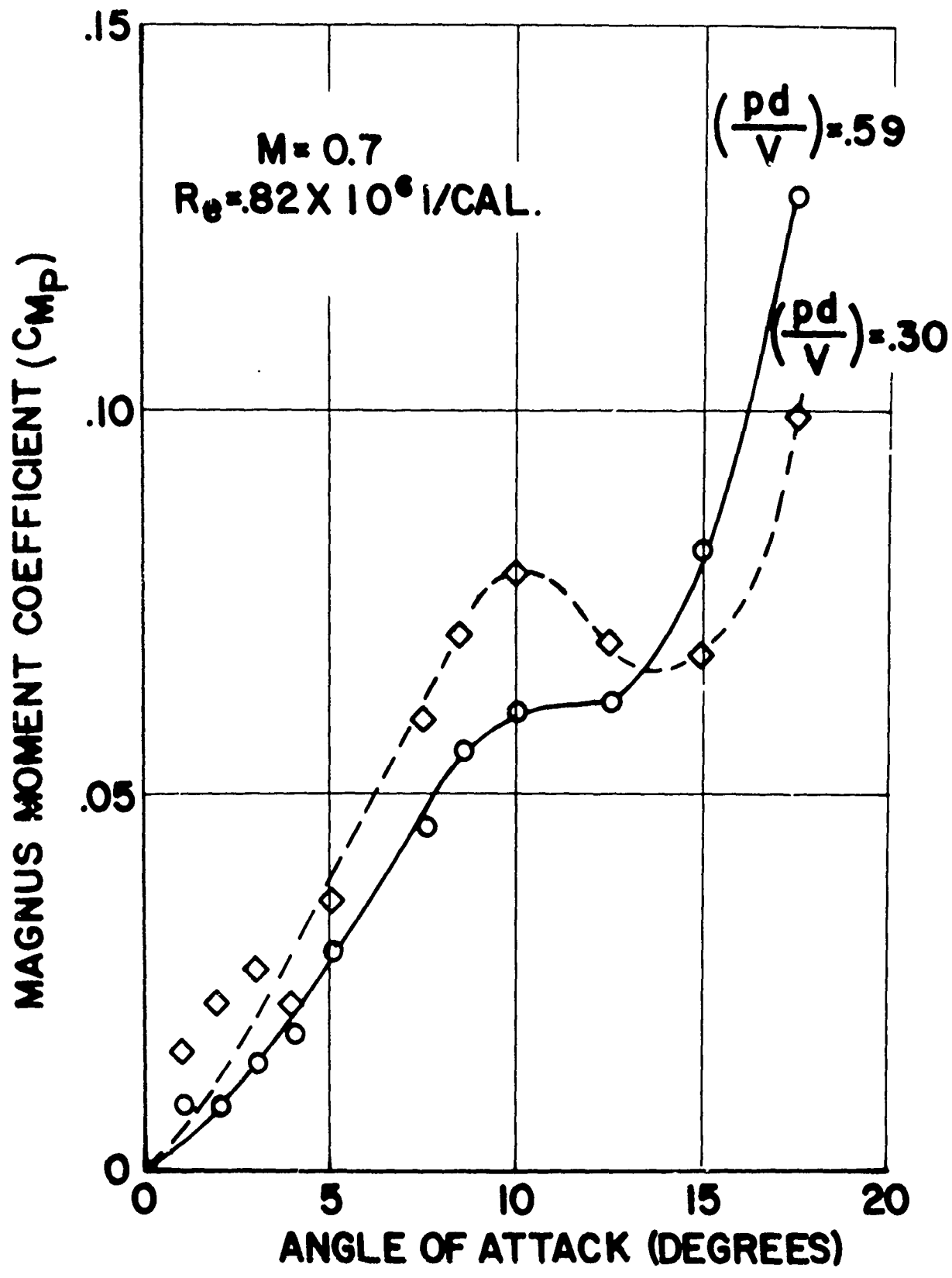


Figure 11. Spin Effect on Magnus Moment Coefficient at Mach Number 0.7 and Test Reynolds Number  $0.82 \times 10^6$  per caliber

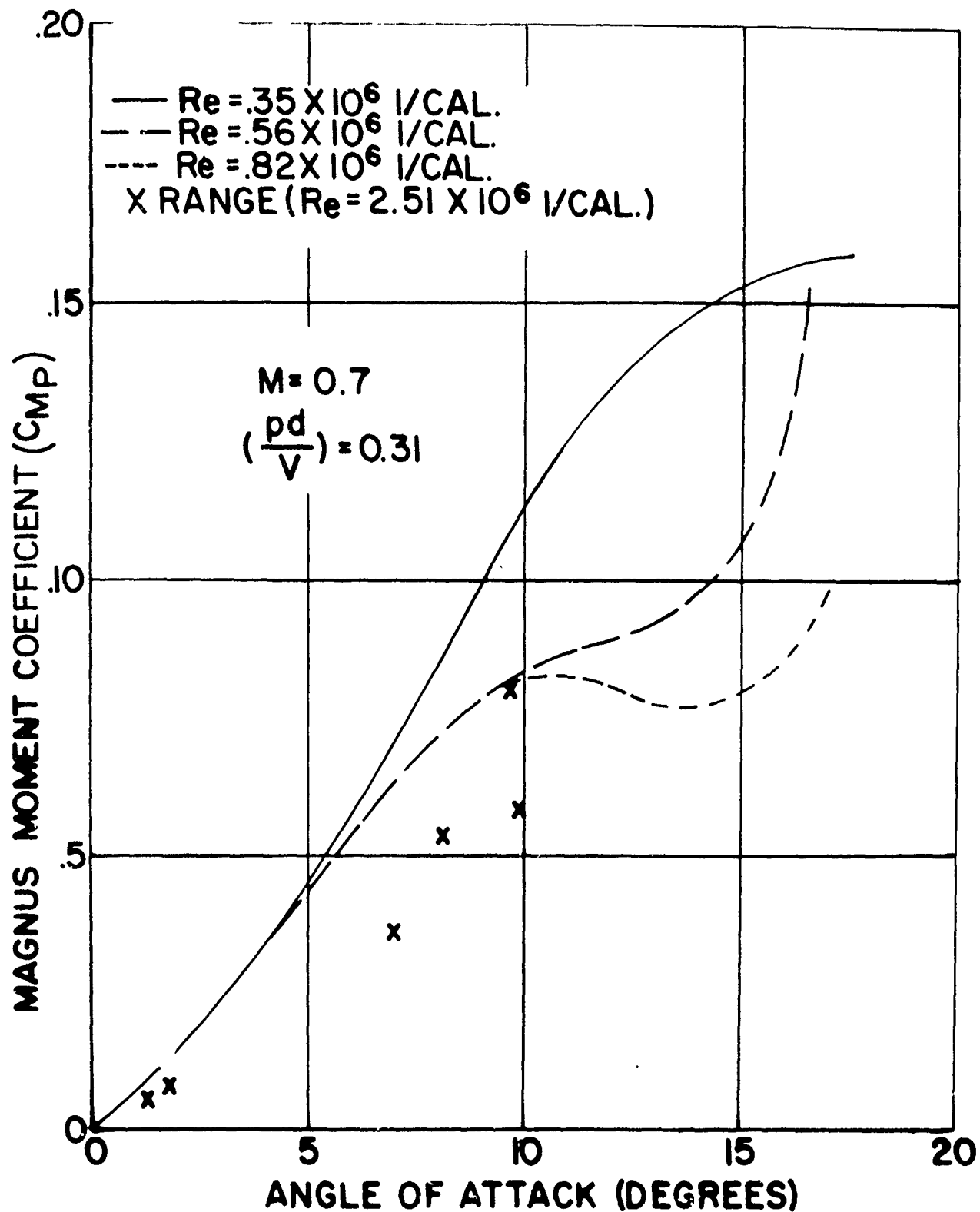


Figure 12. Reynolds Number Effect on Magnus Moment Coefficient at Mach Number 0.7 and Non-dimensional Spin Value 0.31

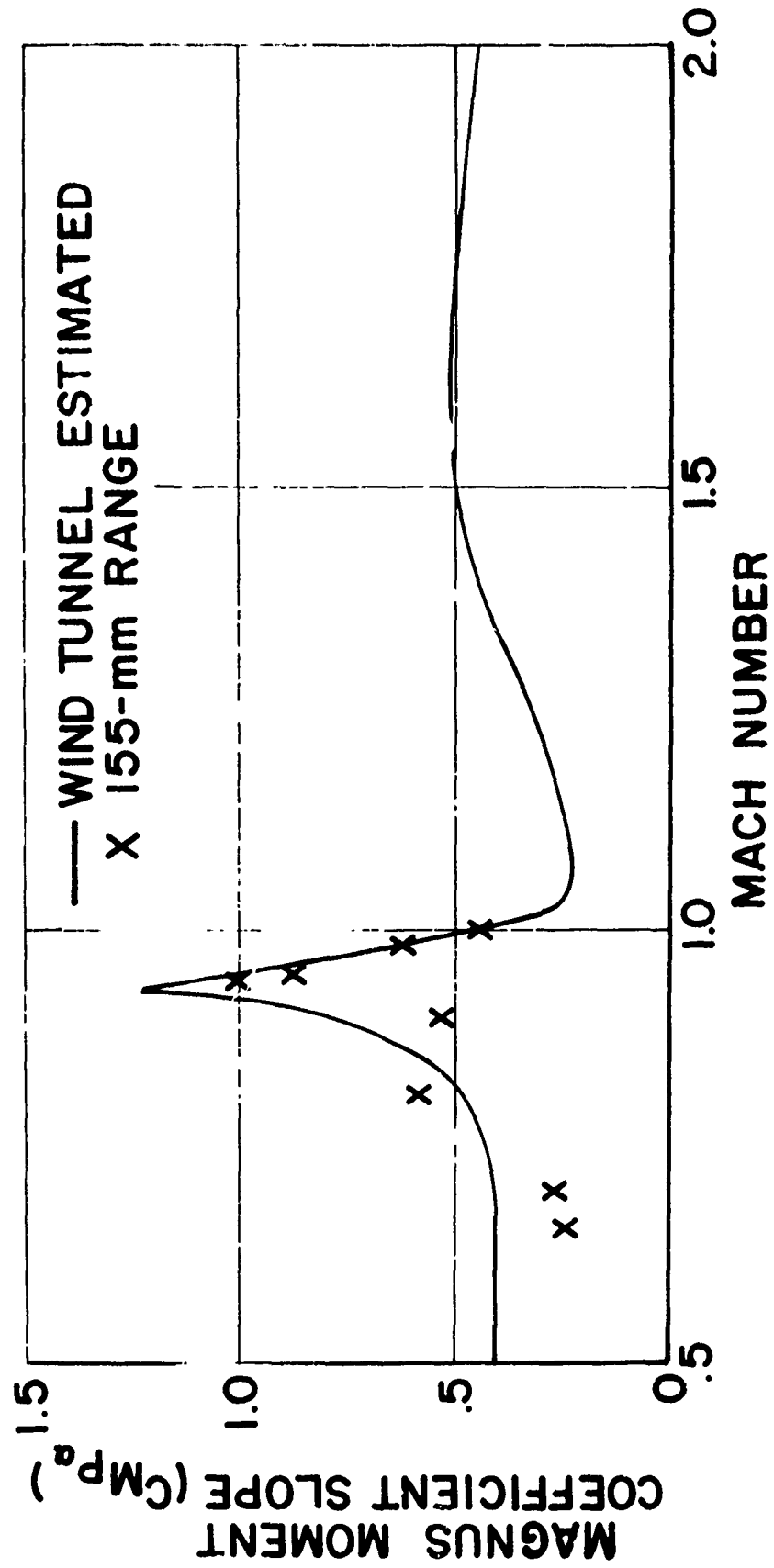


Figure 13. Mach Number Trend of Magnus Moment Coefficient Slope

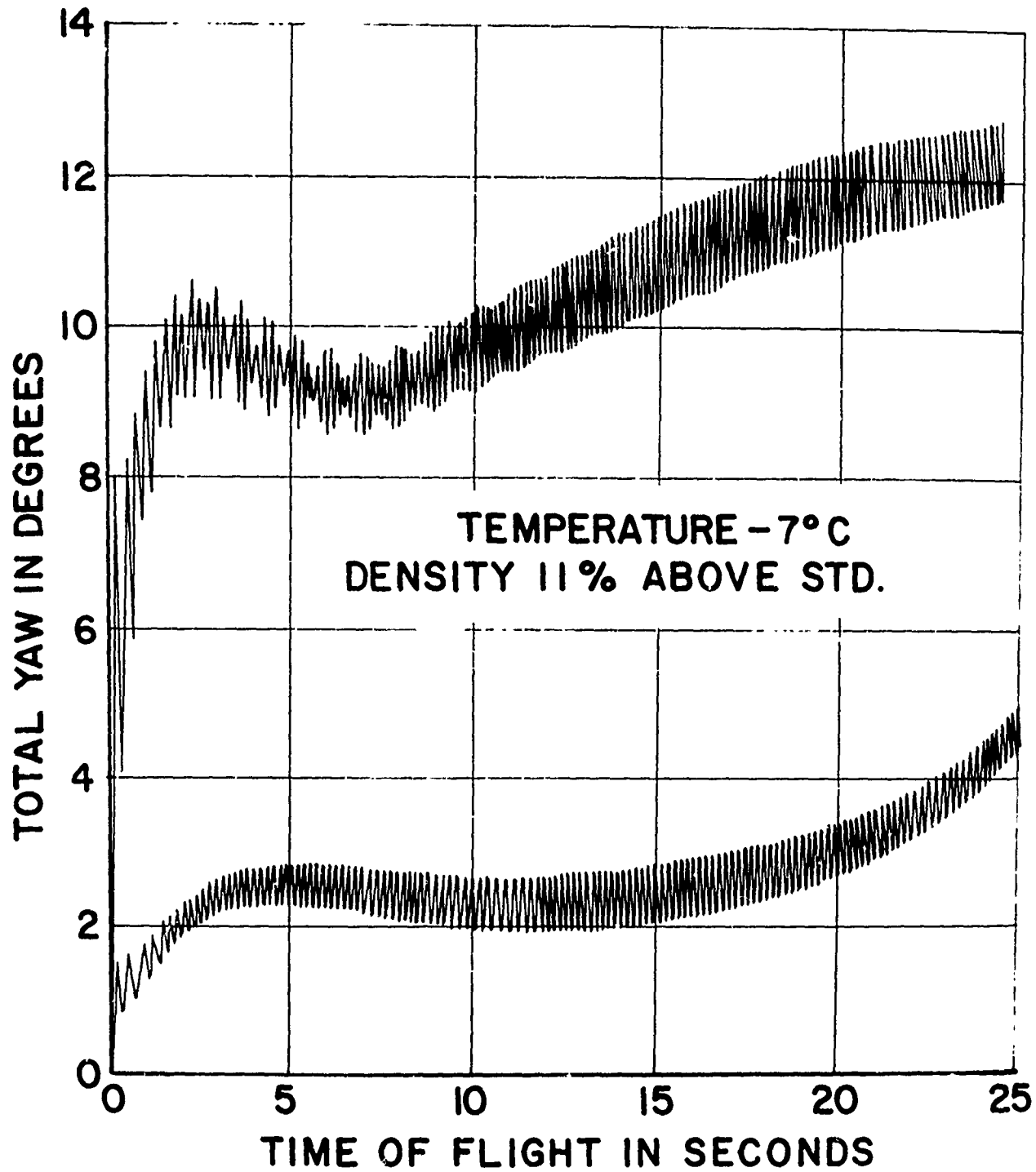


Figure 14. Comparison of Computed Yawing Histories under Aberdeen Proving Ground Environment

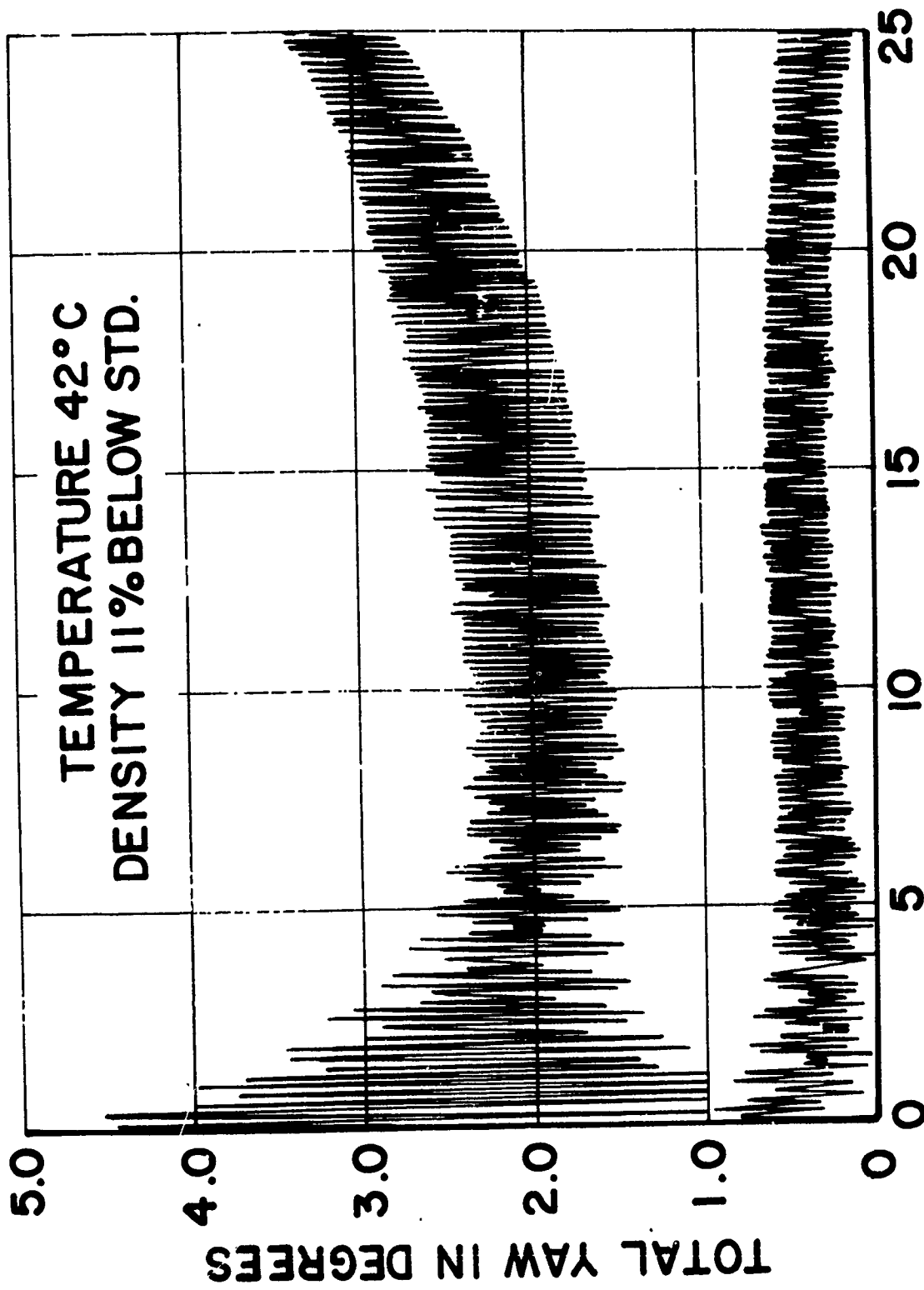


Figure 15. Comparison of Computed Yawing Histories under Yuma Proving Ground Environment

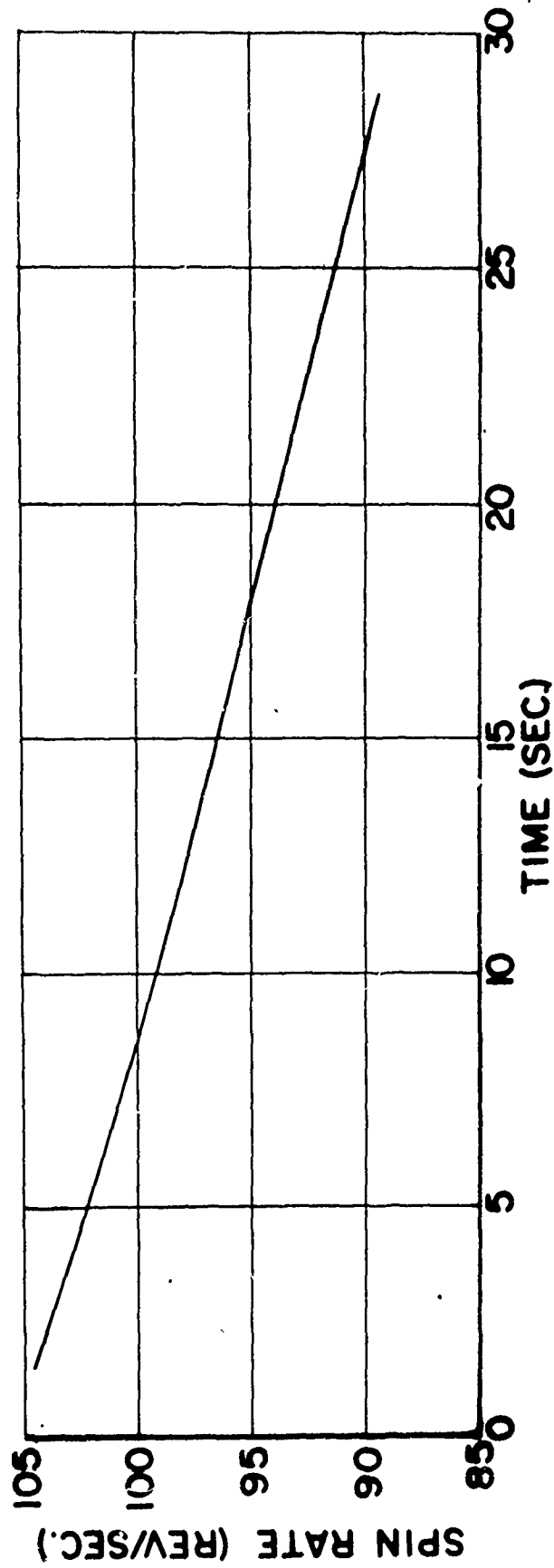


Figure 16. Spin History of a Yawsonde Instrumented Projectile Tested at Wallops Island

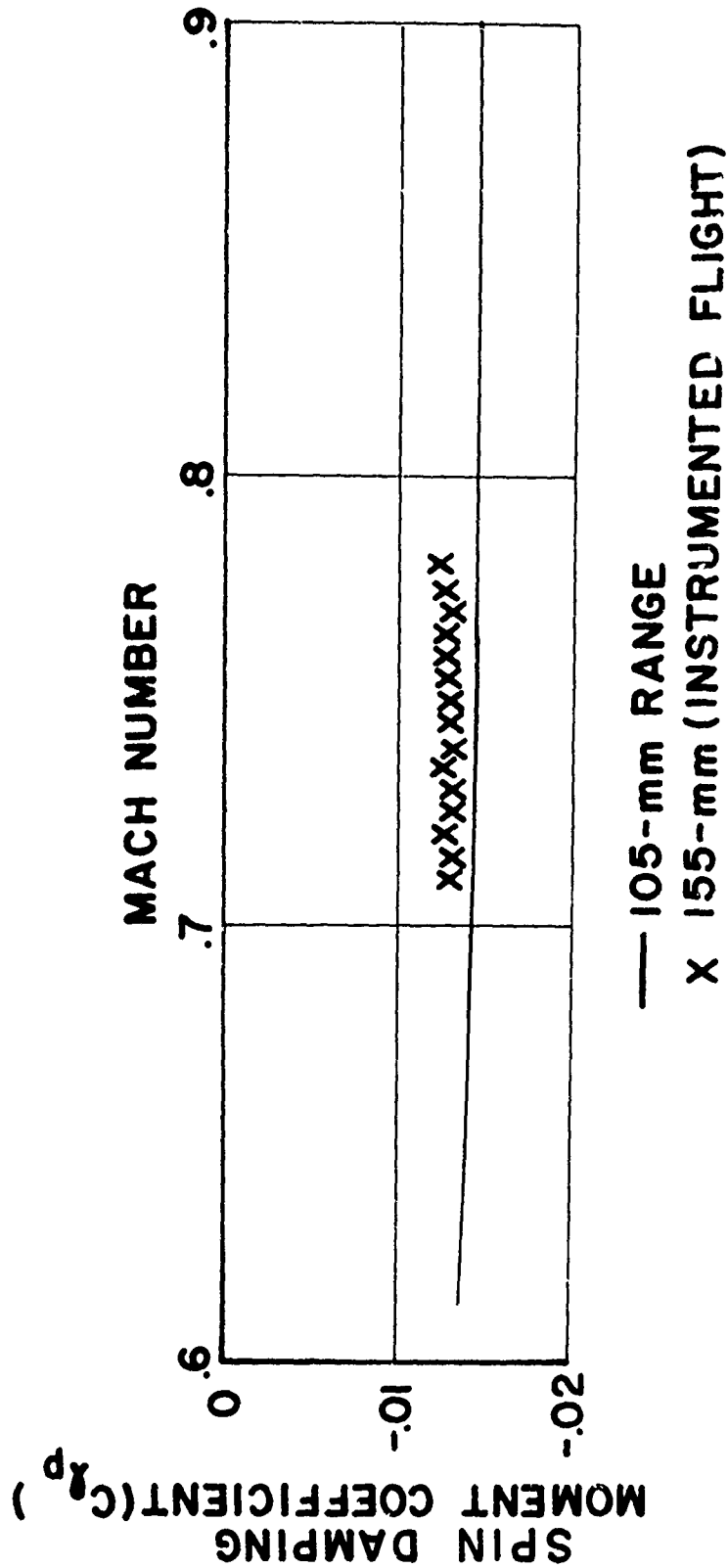


Figure 17. Spin Damping Coefficient Computed from Yawsonde Instrumented Projectile Tests

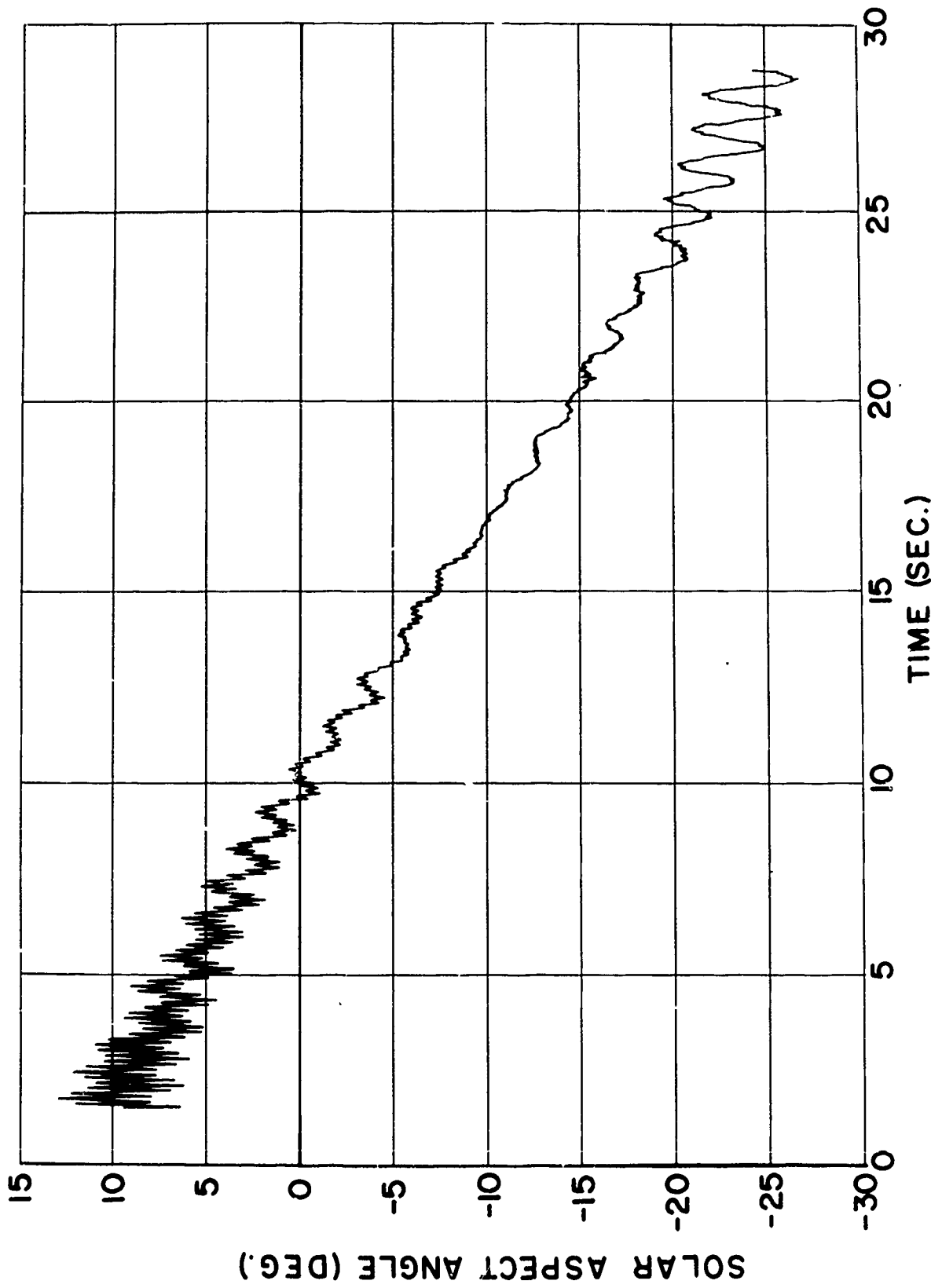


Figure 18. Solar Aspect Angle History of a Yawsonde Instrumented Projectile Tested at Wallops Island

#### REFERENCES

1. W. K. Rogers, Jr., "The Transonic Free Flight Range," Ballistic Research Laboratories Report No. 1044, 1958, AD 200177.
2. J. H. Whiteside, "Interim Report on Projectile, 155mm: HE, XM549," Ballistic Research Laboratories Memorandum Report No. 2165, 1972, AD 894054L.
3. A. S. Platou and G. I. T. Nielsen, "Some Aerodynamic Characteristics of the Artillery Projectile XM549," Ballistic Research Laboratories Memorandum Report No. 2284, 1973, AD 910093L.
4. K. S. Krial and L. C. MacAllister, "Aerodynamic Properties of a Family of Shell of Similar Shape -- 105mm XM380E5, XM380E6, T388 and 155mm T387," Ballistic Research Laboratories Memorandum Report No. 2023, 1970, AD 866610.
5. A. C. Mansfield, G. E. Burt, and T. O. Shadow, "Dynamic Stability Characteristics of the 155mm XM549 Projectile at Mach Numbers from 0.4 to 2.5," ARO Report No. AEDC-TR-7181, 1971.

DISTRIBUTION LIST

<u>No. of Copies</u>	<u>Organization</u>	<u>No. of Copies</u>	<u>Organization</u>
2	Commander Defense Documentation Center ATTN: TDCR Cameron Station Alexandria, Virginia 22314	1	Commander U.S. Army Materiel Command ATTN: AMCRD-DN 5001 Eisenhower Avenue Alexandria, Virginia 22304
1	Director Defense Nuclear Agency ATTN: STRA W.W. Berning Washington, DC 20305	1	Commander U.S. Army Materiel Command ATTN: AMCRD-H 5001 Eisenhower Avenue Alexandria, Virginia 22304
1	Director National Security Agency ATTN: P. W. Waldo, Jr. Fort George G. Meade Maryland 20755	1	Commander U.S. Army Materiel Command ATTN: AMCRD-W 5001 Eisenhower Avenue Alexandria, Virginia 22304
1	Commander U.S. Army Materiel Command ATTN: AMCDL 5001 Eisenhower Avenue Alexandria, Virginia 22304	1	Commander U.S. Army Aviation Systems Command ATTN: AMSAV-E 12th and Spruce Streets St. Louis, Missouri 63166
1	Commander U.S. Army Materiel Command ATTN: AMCRD, MG S. C. Meyer 5001 Eisenhower Avenue Alexandria, Virginia 22304	1	Director U.S. Army Air Mobility Research and Development Laboratory Ames Research Center Moffett Field, California 94035
1	Commander U.S. Army Materiel Command ATTN: AMCRD, Dr. J.V.R. Kaufman 5001 Eisenhower Avenue Alexandria, Virginia 22304	4	Commander U.S. Army Electronics Command ATTN: AMSEL-RD AMSEL-DL SELRA-SMA, M. Bernstein M. Lowenthal Fort Monmouth, New Jersey 07703
1	Commander U.S. Army Materiel Command ATTN: AMCRD-T 5001 Eisenhower Avenue Alexandria, Virginia 22304		
1	Commander U.S. Army Materiel Command ATTN: AMCRD-MT 5001 Eisenhower Avenue Alexandria, Virginia 22304		

PRECEDING PAGE BLANK - NOT FILMED

DISTRIBUTION LIST

<u>No. of Copies</u>	<u>Organization</u>	<u>No. of Copies</u>	<u>Organization</u>
4	Commander U.S. Army Missile Command ATTN: AMSMI-R AMSMI-RBL AMSMI-RST, R. Enpes J. Howell Redstone Arsenal, Alabama 35809	7	Commander U.S. Army Picatinny Arsenal ATTN: SARPA-DR-D, Mr. S. Wasserman Mr. R. Botticelli SARPA-DR-V, Mr. Loeb Mr. D. Mertz Mr. T. Revinus SARPA-AD-D-A-3 Mr. M. Margolin Mr. R. Heredia Dover, New Jersey 07801
2	Commander U.S. Army Missile Command ATTN: AMSMI-RDK Mr. R. Becht Mr. R. Deep Redstone Arsenal, Alabama 35809	1	Commander U.S. Army White Sands Missile Range ATTN: Mr. Webb New Mexico 88002
1	Commander U.S. Army Tank Automotive Command ATTN: AMSTA-RHFL Warren, Michigan 48090	1	Commander U.S. Army Watervliet Arsenal Watervliet, New York 12189
2	Commander U.S. Army Mobility Equipment Research & Development Center ATTN: Tech Docu Cen, Bldg. 315 AMSME-RZT Fort Belvoir, Virginia 22060	1	Commander U.S. Army Safeguard Systems Command Huntsville, Alabama 35804
1	Commander U.S. Army Armament Command Rock Island, Illinois 61202	1	Director U.S. Army Advanced Materiel Concepts Agency 2461 Eisenhower Avenue Alexandria, Virginia 22314
4	Commander U.S. Army Frankford Arsenal ATTN: J8000, Mr. Mitchell K3000, Mr. Fulton J6300, S. Hirshman Mr. J. Capizzi Philadelphia, Pennsylvania 19137	7	Commander U.S. Army Harry Diamond Laboratories ATTN: AMXDO-TI AMXDO-TD, M. Apstein AMXDO-DBC, T. Liss T. Tuccinardi AMXDO-DAC, F. Vrataric AMXDO-DAD, D. Finger AMXDO-DAB, H. Davis Washington, DC 20438

DISTRIBUTION LIST

<u>No. of Copies</u>	<u>Organization</u>	<u>No. of Copies</u>	<u>Organization</u>
1	Commander U.S. Army Materials and Mechanics Research Center ATTN: AMXMR-ATL Watertown, Massachusetts 02172	2	Commander U.S. Naval Weapons Center ATTN: Code 753, Lib Dr. Haseltine China Lake, California 93555
1	Commander U.S. Army Natick Laboratories ATTN: AMXRE, Dr. D. Sieling Natick, Massachusetts 01762	6	Commander U.S. Naval Ordnance Laboratory ATTN: Code 031, Mr. K. Lobb Code 312, Mr. R. Regan Mr. S. Hastings Code 730, Tech Lib Mr. D. Merritt Mr. P. Aronson Silver Spring, Maryland 20910
1	Deputy Assistant Secretary of the Army (R&D) ATTN: Mr. C. L. Poor Washington, DC 20310	3	Director U.S. Naval Research Laboratory ATTN: Tech Info Div Code 7700, Dr. A. Kolb Code 7720, Dr. E. McLean Washington, DC 20390
1	Commander U.S. Army Research Office (Durham) ATTN: CRD-AA-EH Box CM, Duke Station Durham, North Carolina 27706	1	Commander U.S. Naval Weapons Laboratory ATTN: Code GX, Dr. W. Kemper Dahlgren, Virginia 22448
1	Director U.S. Army Advanced Ballistics Missile Defense Agency P. O. Box 1500 Huntsville, Alabama 35809	4	Commander U.S. Naval Weapons Laboratory ATTN: Code GBJ, R. Kapnick E. Ohlmeyer Code TI-3, J. Hurtt Dr. T. Clare Dahlgren, Virginia 22448
1	Director Office of Naval Research ATTN: Mr. S. Curley 495 Summer Street Boston, Massachusetts 02210	3	Commander U.S. Naval Ordnance Station ATTN: Mr. D. Monetta Mr. W. Burnett Dr. Roberts Indian Head, Maryland 20640
3	Commander U.S. Naval Air Systems Command ATTN: AIR-604 Washington, DC 20360	2	ADTC (ADBPS-12) Eglin AFB Florida 32542
3	Commander U.S. Naval Ordnance Systems Command ATTN: ORD-9132 Washington, DC 20360		

DISTRIBUTION LIST

<u>No. of Copies</u>	<u>Organization</u>	<u>No. of Copies</u>	<u>Organization</u>
2	AFATL (DLRA, Mr. F. Burgess; Tech Lib) Eglin AFB Florida 32542	5	Director NASA Ames Research Center ATTN: Mr. D. R. Harrison Mr. T. Canning Dr. D. Kirk Dr. G. T. Chapman Dr. M. Tobak Moffett Field, California 94035
1	AFWL (WLIL) Kirtland AFB New Mexico 87117		
1	AFFDL Wright-Patterson AFB Ohio 45433	1	Director NASA Scientific & Technical Information Facility ATTN: SAK/DL P. O. Box 33 College Park, Maryland 20740
1	ARD (ARIL) Wright-Patterson AFB Ohio 45433		
1	ARL Wright-Patterson AFB Ohio 45433	1	Director National Aeronautics and Space Administration Goddard Space Flight Center ATTN: Tech Lib Greenbelt, Maryland 20771
1	ASD (ASAMCC) Wright-Patterson AFB Ohio 45433		
1	RTD (FDPE, Mr. J. Sedderke) Wright-Patterson AFB Ohio 45433	1	Director National Aeronautics and Space Administration Langley Research Center ATTN: MS 185, Tech Lib Langley Station Hampton, Virginia 23365
1	Environmental Sciences Services Administration ATTN: Code 82.70, J.W. Wright Boulder, Colorado 80301	5	Director National Aeronautics and Space Administration Wallops Station ATTN: Mr. R. Krieger Mr. C. Layton Mr. J. Green Mr. J. Andrew Mr. W. Lord Wallops Island, Virginia 23337
1	Director National Bureau of Standards ATTN: Tech Lib U.S. Department of Commerce Washington, DC 20234		

DISTRIBUTION LIST

<u>No. of Copies</u>	<u>Organization</u>	<u>No. of Copies</u>	<u>Organization</u>
1	Director Jet Propulsion Laboratory ATTN: Tech Lib 4800 Oak Grove Drive Pasadena, California 91103	4	Calspan Corporation ATTN: Library Mr. J. Martin Dr. W. Wurster Dr. G. Skinner P. O. Box 235 Buffalo, New York 14221
2	ARO, Inc. ATTN: Tech Lib Arnold AFS Tennessee 37389	1	Harvard University ATTN: Dept of Aeronautics Cambridge, Massachusetts 02138
1	General Electric Company Armament Department ATTN: Mr. Robert H. Whyte Room 1412 Lakeside Avenue Burlington, Vermont 05401	1	Director Applied Physics Laboratory The Johns Hopkins University 8621 Georgia Avenue Silver Spring, Maryland 20910
5	Sandia Corporation ATTN: Aerodynamics Dept Org 5620, R. Maydew Mr. W. Curry Mr. R. Bentley Mr. O. George P. O. Box 5800 Albuquerque, New Mexico 87115	1	The Johns Hopkins University ATTN: Head of Department of Aeronautics 34th and Charles Streets Baltimore, Maryland 21218
2	California Institute of Technology Aeronautics Department ATTN: Prof H. Liepmann Dr. W. Bekrens Pasadena, California 91102	1	Massachusetts Institute of Technology Department of Aeronautics and Astronautics ATTN: Tech Lib 77 Massachusetts Avenue Cambridge, Massachusetts 02139
1	Guggenheim Aeronautical Laboratory California Institute of Technology ATTN: Tech Lib Pasadena, California 91104	1	Massachusetts Institute of Technology ATTN: Dr. H. P. Greenspan 77 Massachusetts Avenue Cambridge, Massachusetts 02139
		1	Director Guggenheim Aerospace Labs New York University New York Heights New York, New York 10053

DISTRIBUTION LIST

<u>No. of Copies</u>	<u>Organization</u>	<u>No. of Copies</u>	<u>Organization</u>
1	Ohio State University Department of Aeronautical and Astronautical Engineering ATTN: Tech Lib Columbus, Ohio 43210		<u>Aberdeen Proving Ground</u>  Ch, Tech Lib Marine Corps Ln Ofc CO, USALWL CMDR, USATECOM
1	Director Forrestal Research Center Princeton University Princeton, New Jersey 08540		ATTN: AMSTE-BE, Mr. Morrow AMSTE-TA-R, Mr. Wise CMDR, USAEA
1	University of Maryland ATTN: Dr. Y. M. Lynn 5401 Wilkens Avenue Baltimore, Maryland 21228		ATTN: SAREA-R, Mr. A. Flatou SAREA-WGM, Mr. W. Dee Mr. D. Cohen SAREA-DE-WG Mr. J. Jacoby DIR, USAMSAA
2	University of Michigan Department of Aeronautical Engineering ATTN: Dr. A. Kuethe Dr. M. Sichel East Engineering Building Ann Arbor, Michigan 48104		

UNCLASSIFIED

Security Classification

DOCUMENT CONTROL DATA - R & D

(Security classification of title, body of abstract and indexing annotation must be entered when the overall report is classified)

1. ORIGINATING ACTIVITY (Corporate author) U. S. Army Ballistic Research Laboratories Aberdeen Proving Ground, Maryland 21005		2a. REPORT SECURITY CLASSIFICATION Unclassified	
		2b. GROUP	
3. REPORT TITLE VERIFICATION OF GROUND TEST DATA BY INSTRUMENTED FLIGHT TEST OF AN ARTILLERY SHELL			
4. DESCRIPTIVE NOTES (Type of report and inclusive dates)			
5. AUTHOR(S) (First name, middle initial, last name) V. Oskay and J. H. Whiteside of U. S. Army Ballistic Research Laboratories S. Kahn of U. S. Army Picatinny Arsenal			
6. REPORT DATE OCTOBER 1973		7a. TOTAL NO. OF PAGES 46	7b. NO. OF REFS 5
8a. CONTRACT OR GRANT NO. a. PROJECT NO. RDT&E 1T262301A201 c. d.		8b. ORIGINATOR'S REPORT NUMBER(S) BRL MEMORANDUM REPORT NO. 2337	
		8c. OTHER REPORT NO(S) (Any other numbers that may be assigned this report)	
10. DISTRIBUTION STATEMENT Distribution limited to US Government agencies only. Other requests for this document must be referred to Director, USA Ballistic Research Laboratories, ATTN: AMXBR-SS, Aberdeen Proving Ground, Maryland 21005. <i>TS 10 JUN 1974</i>			
11. SUPPLEMENTARY NOTES		12. SPONSORING MILITARY ACTIVITY U. S. Army Materiel Command Washington, D. C. 20315	
13. ABSTRACT Service tests of a new low-drag projectile showed unexpected behavior at intermediate temperatures and low gun elevations where no problems were expected. An extensive test program was initiated to investigate the causes of this behavior. This program included wind tunnel and spark range tests at a wide range of Mach numbers and angles of attack. Given the shell's pitch damping, static, and highly nonlinear Magnus moment coefficients, it was possible to predict its behavior mathematically if the initial pitching rate of the projectile was permitted to vary within the observed limits. Instrumented flight tests verified some of the ground test results although there still remains some unexplained discrepancies in the details of flight behavior. This investigation proved the necessity of a thorough aerodynamic test program if details of a shell's behavior are to be mathematically simulated.			

DD FORM 1473 1 NOV 66

REPLACES DD FORM 1473, 1 JAN 66, WHICH IS OBSOLETE FOR ARMY USE.

UNCLASSIFIED

Security Classification

14	KEY WORDS	LINK A		LINK B		LINK C	
		ROLE	WT	ROLE	WT	ROLE	WT
	data comparison between test sources flight simulation by computer instrumented shell testing data from instrumented shell tests yawsondes flight behavior low drag artillery shell						